Computers in Biology and Medicine 159 (2023) 106897

Contents lists available at ScienceDirect

Computers in Biology and Medicine

journal homepage: www.elsevier.com/locate/compbiomed

A mechanobiological model for tumor spheroid evolution with application to glioblastoma: A continuum multiphysics approach

Ana Carrasco-Mantis [a], Teodora Randelovic [b,c], Héctor Castro-Abril [b,c,d], Ignacio Ochoa [b,c,d], Manuel Doblaré [b,c,d], José A. Sanz-Herrera [a,*]

[a] Escuela Técnica Superior de Ingeniería, Universidad de Sevilla, Spain
[b] Aragón Institute of Engineering Research (I3A), University of Zaragoza, Spain
[c] Aragón Institute of Health Research (IIS), Spain
[d] Centro de Investigación Biomédica en Red en Bioingeniería, Biomateriales y Nanomedicina (CIBER-BBN), Spain

ARTICLE INFO

Keywords:
Cellular spheroid
Glioblastoma
Mechanobiology
Numerical simulation
Finite element method

ABSTRACT

Background: Spheroids are in vitro quasi-spherical structures of cell aggregates, eventually cultured within a hydrogel matrix, that are used, among other applications, as a technological platform to investigate tumor formation and evolution. Several interesting features can be replicated using this methodology, such as cell communication mechanisms, the effect of gradients of nutrients, or the creation of realistic 3D biological structures. The main objective of this work is to link the spheroid evolution with the mechanical activity of cells, coupled with nutrient consumption and the subsequent cell dynamics.

Method: We propose a continuum mechanobiological model which accounts for the most relevant phenomena that take place in tumor spheroid evolution under in vitro suspension, namely, nutrient diffusion in the spheroid, kinetics of cellular growth and death, and mechanical interactions among the cells. The model is qualitatively validated, after calibration of the model parameters, versus in vitro experiments of spheroids of different glioblastoma cell lines.

Results: Our model is able to explain in a novel way quite different setups, such as spheroid growth (up to six times the initial configuration for U-87 MG cell line) or shrinking (almost half of the initial configuration for U-251 MG cell line); as the result of the mechanical interplay of cells driven by cellular evolution.

Conclusions: Glioblastoma tumor spheroid evolution is driven by mechanical interactions of the cell aggregate and the dynamical evolution of the cell population. All this information can be used to further investigate mechanistic effects in the evolution of tumors and their role in cancer disease.

1. Introduction

Spheroids are increasingly used in the recent years as an enabling biological platform to study tumor formation, evolution, as well as to study cancer treatments [1]. Spheroids are clusters of cells, eventually cultured within a hydrogel matrix that mimics the extracellular matrix, which show a quasi-spherical morphology in vitro [2]. Even though spheroids lack the enormous complexity of tumor tissues, they are useful in vitro models as they are able to replicate several important features of solid tumors. In particular, communication mechanisms and cell differentiation have been observed in spheroids [3]. Also, the high cell density and compaction in larger spheroids induce areas that suffer hypoxia and gradients of nutrients, as the diffusion within the structure is limited, becoming a good surrogate for these effects that happen in reality [4]. Moreover, the 3D environment of the spheroid, versus 2D, allows a better understanding of the mechanisms of cellular communication and signaling, both autocrine and paracrine, and the different types of cell migration stimuli, such as chemotaxis, durotaxis, electrotaxis and haptotaxis [5]. Tumor heterogeneity (intertumoral or intratumoral) is another important characteristic, related to resistance, which can be also reproduced by spheroids [6].

From an in vitro point of view, spheroids have been used to study the mechanisms of cell differentiation, cell contact and the different cell phenotypes that give rise to different regions within the spheroid [7]. Furthermore, Friedrich et al. [8] developed platforms to study anti-cancer treatments in spheroids. Nath and Devi [9] presented several spheroid generation techniques and assays for their characterization. On the other hand, Mark et al. [10] studied the relationship between the cellular mechanics of the spheroid and the deformation of the extracellular matrix; and Ayuso et al. [11] established that spheroids

* Correspondence to: Camino de los descubrimientos s/n, 41092 Seville, Spain.
E-mail address: jsanz@us.es (J.A. Sanz-Herrera).

https://doi.org/10.1016/j.compbiomed.2023.106897
Received 11 November 2022; Received in revised form 9 February 2023; Accepted 9 April 2023
Available online 18 April 2023

represent a good tool in the study of migration by chemotaxis, the main mechanism of cell migration. In another study, Guillaume et al. [12] suggested that the stresses that originate in a spheroid during its growth affect its physical properties and therefore the response to treatment. Wu et al. [13] developed microfluidic devices for the study of chemotaxis, through the generation of chemical gradients in both simple and complex environments, and studied chemotaxis as a function of the cell type. The devices designed by Cheng et al. [14] allow a quick reconfiguration for use in different applications, including the analysis of tumor first development and evolution. Ayuso et al. [15] performed a protocol for the confinement of the gel in microfluidic chips and, subsequently [16], they were able to reproduce the complex tumor environment in these platforms. Fatehullah et al. [17] presented a generation of organoids from biopsies performed on tumor tissues and their subsequent cultivation in hydrogels, which constitute a novel test in the study of pathologies and treatments.

From an in silico perspective, Xue et al. [18] developed a continuum model to investigate the relationship between biology, chemistry and mechanics in the evolution of tumor spheroids by treating the tumor as a porous system. They highlighted the importance of nutrient transport and mechanical stresses in growth. The model was validated with data taken from the literature. Also, Mascheroni et al. [19] presented a continuum tumor spheroid growth model whose equations were developed according to the porous media theory. This study also performed experiments with the U-87 MG tumor line, including both free and pressurized growth. However, the diffusion of nutrients into the different cell types of the spheroid was not considered. Greenspan [20] developed a continuum model to analyze growth of a colony of cells, which compares to the movement of an incompressible fluid in a membrane of variable size. Growth was considered to be influenced by a surface tension force and by the diffusion of nutrients in this work. Nonetheless, the analysis was not conducted for spheroids, and the results were not compared with experiments. Byrne and Chaplain [21] showed that nutrient concentration at the spheroid boundary is not constant, but follows the Gibbs–Thomson relationship, which states that the local curvature at the edge of the spheroid influences this concentration, carrying out a mathematical description of this phenomenon. The results were not validated in this study. Furthermore, Chen et al. [22] proposed a model that analyzes how the mechanics of the elastic and isotropic extracellular medium affects tumor evolution, but it does not model the mechanical interactions of the cells in the spheroid. The authors stated that when a spheroid grows, it exerts a pressure on the medium, which in turn exerts a stress on the spheroid contour. In addition, they performed an experimental validation of their model, based on results found in the literature. Ambrosi and Mollica [23] described the growth of a tumor spheroid, influenced by nutrient diffusion and biochemical factors, considering the same number of particles at each instant of time and justifying growth as an increase of mass of the particles but not on their number. Hence, the dynamics of cellular proliferation and death was not considered, and an experimental validation of the model was not conducted. In addition, Ambrosi and Mollica [24] studied the growth of a spheroidal tumor as a soft tissue and highlighted the need to know the history of inhomogeneous mass increase. The authors developed a mathematical model for the experiments performed by other authors. In a different study, Ambrosi et al. [25] assumed that the spheroid behaves as a poroelastic material whose growth is influenced by the stress applied on its boundary. The authors also studied the presence of residual stresses in the spheroid. In order to experimentally validate their model, they based their work on previous existing studies in the literature. Fraldi and Carotenuto [26] carried out a poroelastic model in which an inelastic growth derived from a Volterra/Lotka type interaction between different cell types occurs. However, nutrient diffusion was not considered in this work. Additionally, Bull et al. [27] recently proposed a discrete (agent-based) approach to model the dynamics of cells in spheroids, accounting for the diffusion of nutrients and oxygen from the medium to the interior of the spheroid, which determines the cellular actions of proliferation, differentiation and cell death. In the same context, Amereh et al. [28] presented a mathematical model of tumor formation in spheroids based on reaction–diffusion equations.

With regard to mathematical mechanobiological models, there is a vast literature on different methodologies and mathematical approaches to study in silico the effect of mechanics in biological processes. To cite a few, Perfahl et al. [29] developed a vasculogenesis model which considers the application of forces through the interaction of cells with their neighbors and with the extracellular environment, obtaining a vascular network as results of the simulations. Ayensa-Jiménez et al. [30], described a mathematical model of cell dynamics, growth and death, in a microfluidic device with application to glioblastoma evolution. Laird [31] performed a mathematical model of tumor proliferation with different growth stages. Furthermore, Pettet et al. [32] implemented a mathematical model of cell migration in spheroids, where chemotaxis plays an important role. Lu and Kang [33] analyzed how hypoxia-inducing factors are related to increased treatment failure and mortality, while Curtis and Seehar [34] studied the relationship between cell mechanics and proliferation, concluding that compression increases proliferation. Moreo et al. [35] carried out a predictive mechanosensing model that explains the interaction between the cell cytoskeleton and the extracellular matrix through focal adhesions. In addition, they also studied cell migration by modeling the evolution of cell concentration from a continuum point of view. Furthermore, Sanz-Herrera et al. [36] studied how, through contractile forces, the contact between a cell and the substrate occurs when it shows a curvature, analyzing the influence of microfilament bending and the initial shape of the substrate. Huang and Ingber [37] described how through integrins, focal adhesions and Rho/ROCK signaling that enables cellular contractility, a mechanistic process of autocrine cell communication important in cancer development, occurs. Additionally, Nagelkerke et al. [38] highlighted the role of mechanics in cancer development, describing several processes, including activation of the Rho family of proteins, involved in intracellular contractility of the cytoskeleton.

Our application is devoted to analyze glioblastoma spheroids. Glioblastoma is the most malignant brain tumor, with a life expectancy after the standard treatment (surgery plus radio and/or chemotherapy) of about 14 months from diagnosis [39]. It originates in the glial cells and its initial evolution is controlled by thrombosis, hypoxia, cell migration events that occur successively [40] and is characterized by microvascular hyperplasia and necrosis. The area where the latter takes place (necrotic core), is usually surrounded by a high cell density, known as ‘pseudopalisade’. The hypoxic tissue (more resistant than a healthy one [41]) increases tumor glycolysis to provide energy to the cell, promotes angiogenesis, that is the creation of blood vessels and nourishes the tumor invasion and metastasis by the action of hypoxia-inducible factors [33].

In this article, we develop a phenomenological mechanobiological model to investigate the in vitro evolution of suspended glioblastoma spheroids. Compared to previous existing models in the literature, our multiphysics approach describes the evolution of spheroids from the internal mechanical activity of cells in response to nutrient stimuli in the microenvironment in a continuous way. Therefore, the model takes into consideration the main physics observed during the process, such as nutrient diffusion within the spheroid, dynamics of cellular growth and death, and mechanical interactions of cells including computation of biomechanical forces. These latter forces present at the cellular level may have an external origin or may be generated by the cells themselves. They play a fundamental role in maintaining homeostasis in the organism. They can also contribute to the development of pathologies, such as tumor progression, by increasing the rigidity of the extracellular matrix or modifying the flow of interstitial fluid in the matrix [42]. In this work, we test how biomechanical stresses and deformations, generated at the cellular level, influence the organization and morphology

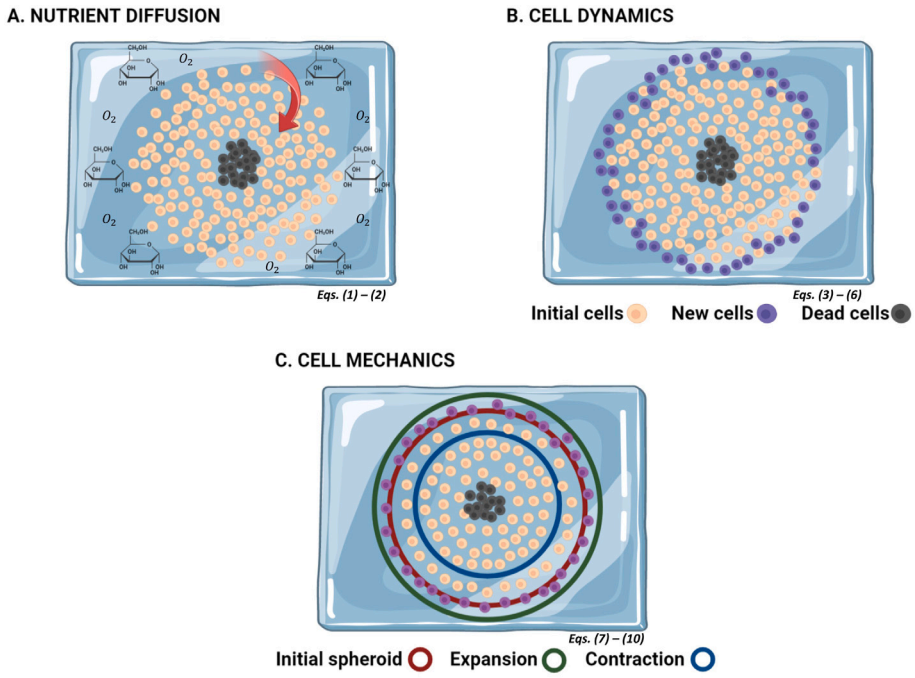

Fig. 1. Multiphysics model: Schematics of the different physics considered in the modeling of suspended spheroid evolution. *Source:* Figure created with BioRender.com.

Table 1
Multiphysics mechanobiological model quantities.

Symbol	Description	Units
$c(\mathbf{x},t)$	Nutrient concentration in the spheroid domain	$\frac{mol}{mm^3}$
$n(\mathbf{x},t)$	Cell concentration in the spheroid domain (superscript g-growth, d-death)	$\frac{cell}{mm^3}$
$\varepsilon^T(\mathbf{x},t)$	Total strain at a material point of the spheroid	–
$\varepsilon^{el}(\mathbf{x},t)$	Elastic strain at a material point of the spheroid (passive component)	–
$\varepsilon^{cell}(\mathbf{x},t)$	Cell strain at a material point of the spheroid as a consequence of internal cell contractility (active component)	–
$\sigma(\mathbf{x},t)$	Stress at a material point of the spheroid as a consequence of cell contractility	Pa

Table 2
Model parameters.

Symbol	Description	Units
c_0	Nutrient concentration in the spheroid domain at time 0	$\frac{mol}{mm^3}$
c_Γ	Nutrient concentration on the spheroid boundary	$\frac{mol}{mm^3}$
k_c	Coefficient of nutrient diffusion from the medium to the spheroid	$\frac{mm^2}{min}$
r	Nutrient consumption rate	$\frac{mol}{cell \cdot min}$
n_0	Cell concentration in the spheroid domain at time 0	$\frac{cell}{mm^3}$
c_n	Nutrient concentration threshold for cells to survive and grow	$\frac{mol}{mm^3}$
c_{sat}	Nutrient concentration saturation value which defines the maximum rate level achieves by cells to divide and grow	$\frac{mol}{mm^3}$
k_d	Cell death rate	$\frac{mm^3}{mol \cdot min}$
k_g	Cell growth rate	$\frac{mm^3}{mol \cdot min}$
n^*	Cell concentration from which cell contractility changes from compression to expansion	$\frac{cell}{mm^3}$
k_e	Cell expansion coefficient as consequence of cell forces exerted by the cytoskeleton machinery	$\frac{mm^3}{cell}$
α	Shape factor coefficient of nutrients in the suspension experiment	$\frac{mol}{cell \cdot min}$

of the tumor spheroids. The overall continuum model was discretized in time and is formulated in the updated Lagrangian configuration for each time step, being spatially discretized by means of the finite element method. The model permits to predict the nonlinear evolution of the spheroid along time, in terms of a number of model parameters. This dependence is investigated in a parametric analysis of the model.

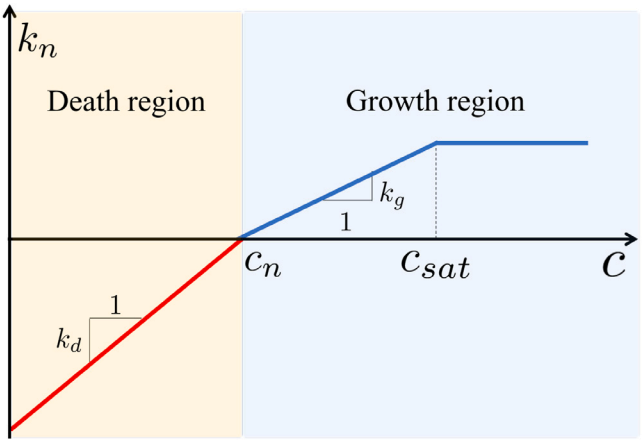

Fig. 2. Cellular growth/death kinetics represented as a function of the nutrient concentration.

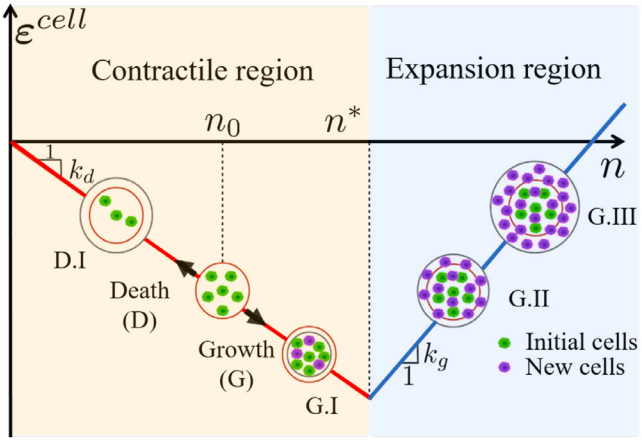

Fig. 3. Active cell's contractility/expansion deformation model as a function of the cell concentration, for death (D) and growth (G) fates. n^* is a model parameter that represents the concentration level for which a new daughter cell cannot be accommodated within the reference volume. n_0 represents the initial concentration of cells.

Finally, two experimental tests were designed *ad-hoc* in this study to qualitatively validate the proposed model. Specifically, the evolution of 1000-cell spheroids of glioblastoma cell lines U-251 MG and U-87 MG were performed and recorded. The model fits the observed trends in the experiments for a set of calibrated parameters, suggesting that the implemented physics can explain the observed behavior. In particular, it is concluded that spheroid growth or shrinking is the result of the mechanical interplay of cells driven by cellular evolution.

The paper is organized as follows: first the experimental setup and the mathematical model are introduced in Sections 2–4. The numerical implementation of the model is elaborated in Section 5, and the parametric analysis is presented in Section 6.1. The validation of the proposed model versus the obtained experimental results is described in Section 6.2. Finally, the discussion of the results and main derived conclusions are drawn at the end of the paper.

2. Experimental setup

Glioblastoma cell lines, U-251 MG and U-87 MG, were purchased from Sigma Aldrich and cultured in high glucose Dulbecco's modified Eagle's medium (DMEM; Lonza BE12-614F), supplemented with 10% fetal bovine serum (FBS; Sigma Aldrich F7524), 2 mM L-glutamine (Lonza 17-605C) and penicillin/streptomycin (Lonza 17-602E). Cell cultures were maintained at 37 °C within a humidified TEB-1000 incubator (EBERS Medical Technology) with 5% CO_2. Spheroids were generated by hanging drop method. Cells were trypsinized and resuspended in growth medium supplemented with 20% methylcellulose solution to reach the concentration of 40 000 cells/mL. In order to form 1000-cell spheroids, 25 uL drops were placed on the lid of a Petri dish. The bottom part of the dish was filled with distilled water to prevent evaporation. Plates were placed within the incubator and left for 48 h to assure spheroid formation. Afterwards, spheroids were transferred to growth medium in suspension 96 well plates (Sarstedt 83.3925.500) treated with anti-adherence solution (Stemcell 07010). Their behavior was followed by phase contrast microscopy (Nikon TiE) during two weeks. Images were analyzed with a Fiji plugin SpheroidJ, which allows automated quantification of the spheroid area [43]. Growth curves were obtained by normalizing those values to the area that spheroids occupied at the beginning of the experiment (day 0).

3. Mathematical model

The proposed mathematical model considers the main phenomena that take place in suspended spheroid evolution, according to experimental observations. In particular, spheroid size evolution is considered to be mainly determined by the proliferation of cells as well as the contractile activity exerted by cells [11,44]. Moreover, nutrient diffusion within the spheroid enhances the dynamics of cells [44], whereas lack of nutrients promotes the formation of a necrotic core in the spheroid [11].

According to the referred evidences the physics assumed by the model are fundamentally three. First, diffusion of soluble substances in the medium, such as nutrients and oxygen, to the spheroid interior. Second, cellular activity and dynamics in terms of proliferation and death, which in turn determine spheroid growth or shrinking evolution from the initial state. Finally, we model cellular contractility and mechanical interactions of cell organization in the spheroid. A spherical geometry of the spheroid is assumed, similar to other works [18,25,26]. Furthermore, as main assumptions, we consider that (i) cell dynamics depends on nutrient concentration and (ii) volume variation of the spheroid is related to cell contractility and concentration. The overall model turns into a mechanobiological and multiphysics coupled approach which is presented in a dimensionless fashion in Section 4. The schematics of the different physics of the model can be seen in Fig. 1. Model quantities and parameters are shown in Tables 1 and 2, respectively. The model is also elaborated in a numerical framework in Section 5.

3.1. Nutrient diffusion

We consider that soluble substances in the medium diffuse towards the spheroid core, leading to nutrient supply to interior cells (see Fig. 1A). Therefore, nutrients (considering nutrients as oxygen and glucose concentration) are assumed, as a first approach, to follow a *Fickean* diffusion model, analogously to other works in a similar context [34,45–47]:

$$\begin{aligned} &\frac{\partial c}{\partial t} = k_c \nabla^2 c - r \cdot n \quad \text{in} \quad \Omega(\mathbf{x}, t) \\ &c(\mathbf{x}, 0) = c_0 \quad \text{in} \quad \Omega(\mathbf{x}, 0) \\ &c(\mathbf{x}, t) = f(\mathbf{x}, t) \quad \text{in} \quad \Gamma_b(\mathbf{x}, t) \end{aligned} \tag{1}$$

The right-hand side of Eq. (1)a also includes a second (source) term which accounts for the consumption rate of nutrients by cells. k_c is the diffusion coefficient of the spheroid aggregation, r is the rate of nutrient consumption by cells, and c_0 the initial concentration of nutrients within the spheroid. Ω represents the domain and Γ_b the contour of the spheroid. On the other hand, the function f represents

Table 3
Dimensionless values of the model parameters for the parametric analysis.

Parameter	Reference value	Lowest value	Highest value
$\tilde{k}_c$	0.01	0.01	0.01
$\tilde{r}$	$1 \cdot 10^{-2}$	$5 \cdot 10^{-3}$	$2 \cdot 10^{-2}$
$\tilde{k}_d$	$1.5 \cdot 10^{-4}$	$0.75 \cdot 10^{-4}$	$3 \cdot 10^{-4}$
$\tilde{k}_g$	$1.5 \cdot 10^{-4}$	$0.75 \cdot 10^{-4}$	$3 \cdot 10^{-4}$
$\tilde{k}_{ed}$	$4 \cdot 10^{-2}$	$2 \cdot 10^{-2}$	$8 \cdot 10^{-2}$
$\tilde{k}_{eg}$	$4 \cdot 10^{-2}$	$2 \cdot 10^{-2}$	$8 \cdot 10^{-2}$
$\tilde{n}^*$	2	1	4
$\tilde{c}_n$	0.5	0.5	0.5
$\tilde{c}_{sat}$	0.9	0.9	0.9

the consumption of nutrients available in the suspension experiment, defined as:

$$\begin{aligned} &\frac{\partial f}{\partial t} = -\alpha \cdot n \quad \text{in} \quad \Gamma_b(\mathbf{x}, t) \\ &f(\mathbf{x}, 0) = c_\Gamma \quad \text{in} \quad \Gamma_b(\mathbf{x}, 0) \end{aligned} \tag{2}$$

with α a factor (shape) coefficient which accounts for the amount and availability of nutrients and configuration of the suspension experiment for diffusion of nutrients. This coefficient is introduced as a correction factor to the full and plenty availability of nutrients hypothesis in the experiment. c_Γ represents the nutrient concentration in the suspension at the initial time of the analysis. Note that, according to Eq. (2), in our model, nutrient concentration may become very low (even negative) in the medium for large time t. Indeed, this behavior is aligned with experimental observations where a recharging/refreshing protocol is needed before complete depletion of nutrients within the medium. This experimental issue can be properly introduced in our model by assuming an update of the function f at certain time points. Of course, negative concentrations do not have any biophysical meaning so our solution would not be valid under this situation, as the complete depletion of nutrients would have been achieved before.

In a different way, Mascheroni et al. [19], alternatively to a Fickean diffusion as considered in Eq. (1), established a mass exchange for nutrient consumption by tumor cells; and Ambrosi et al. [25] compared spheroid diameter with nutrient penetration length to differentiate between volumetric or surface growth.

3.2. Cell dynamics

Spheroid growth or decrease is ultimately depends on the dynamics of the cellular activity (see Fig. 1B). Therefore, the dynamics of cellular growth/death is represented, similar to other works [31,54,55], by means of the following first order differential equation:

$$\begin{aligned} &\frac{\partial n}{\partial t} = k_n(c) \cdot n \quad \text{in} \quad \Omega(\mathbf{x}, t) \\ &n(\mathbf{x}, 0) = n_0 \quad \text{in} \quad \Omega(\mathbf{x}, 0) \end{aligned} \tag{3}$$

In Eq. (3), and as a simplification of other models [30,33,56], the kinetics of cellular growth/death is characterized by the function $k_n(c)$, which is assumed to be dependent of the nutrient concentration [30]. $k_n(c)$ is the function shown in Fig. 2, where two regions can be identified: (i) a cell death (or dormancy) region which appears for low nutrient concentration, and (ii) a cell growth zone for high levels of nutrients. Both regions are regulated by a threshold parameter c_n, which represents the homeostatic level of nutrients in cell's activity. We consider a linear model for k_n for both death and growth regions, finishing this latter with a constant region after a certain saturation level of nutrients c_{sat}.

Therefore, Eq. (3) can be split into two different conditions for death and growth dynamics as follows:

$$\begin{aligned} &\frac{\partial n^d}{\partial t} = -k_d \cdot (c_n - c) \cdot n \quad \text{if} \quad c \le c_n \quad \text{in} \quad \Omega(\mathbf{x}, t) \\ &n^d(\mathbf{x}, 0) = 0 \quad \text{in} \quad \Omega(\mathbf{x}, 0) \end{aligned} \tag{4}$$

$$\begin{aligned} &\frac{\partial n^g}{\partial t} = k_g \cdot (c - c_n) \cdot n \quad \text{if} \quad c > c_n \quad \text{in} \quad \Omega(\mathbf{x}, t) \\ &\frac{\partial n^g}{\partial t} = k_g \cdot (c_{sat} - c_n) \cdot n \quad \text{if} \quad c > c_{sat} \quad \text{in} \quad \Omega(\mathbf{x}, t) \\ &n^g(\mathbf{x}, 0) = 0 \quad \text{in} \quad \Omega(\mathbf{x}, 0) \end{aligned} \tag{5}$$

where k_d and k_g represent death and growth constants, and the superscripts mean d (death) and g (growth), respectively. Finally, the total cell concentration can then be computed as,

$$n(\mathbf{x}, t) = n_0 + n^g(\mathbf{x}, t) + n^d(\mathbf{x}, t) \tag{6}$$

Otherwise, Ambrosi and Mollica [23], in place of cell proliferation and death, stated that the increase in the size of the spheroid is due to an increase in the size of the particles that initially make it up. Bull et al. [27], assumed that cell proliferation and death depend on cell cycle times in their agent-based modeling.

3.3. Cell mechanics

The spheroid is assumed to be subjected to the contractile activity of cells (see Fig. 1C). This phenomenon is modeled by distinguishing between passive and active components of the cytoskeleton. In particular, contractile forces are implemented as an internal active deformation, i.e. contractility, similar to other existing models of (continuum) cytoskeletal behavior [35,36,57]. For the sake of simplicity of our numerical framework, we will use an updated Lagrangian configuration to solve the equations above. Therefore, a small strains formulation (linearized for time t around the current configuration $\Omega(\mathbf{x}, t)$) is applied to describe the cell mechanical interactions in the spheroid for each small time step. Moreover, we assume a linearly elastic and isotropic constitutive relation between stress and strain around the current configuration. Then, for a material point $\mathbf{x}$ which represents a certain cell concentration, the overall deformation $\boldsymbol{\varepsilon}^T$ is the contribution of the elastic deformation (ε^{el}) of the passive component of the cell's cytoskeleton, plus the deformation due to the internal cell contractility $\boldsymbol{\varepsilon}^{cell}$. The interpretation of this strain measure is the logarithmic or Hencky strain, so the considered constitutive model is assumed to be dependent on this metric. This is a natural way of describing constitutive stress–strain relations that has been used in a

Table 4
Values of the calibrated model parameters and bibliographic range.

Parameter	Value (U-251 cells)	Value (U-87 cells)	Bibliographic data	Bibliographic data	Units
k_c	0.0011	0.0016	$[3.96 \cdot 10^{-8}; 0.3]$	[39,48]	$\frac{mm^2}{min}$
r	$2.9777 \cdot 10^{-10}$	$4.9182 \cdot 10^{-8}$	$[2.4 \cdot 10^{-15}; 0.045]$	[49,50]	$\frac{mol}{min \cdot cell}$
k_d	$5 \cdot 10^{-6}$	$5 \cdot 10^{-4}$	$[2.73 \cdot 10^{-5}; 3.53 \cdot 10^{-4}]$	[39,51]	$\frac{mm^3}{mol \cdot min}$
k_g	$5 \cdot 10^{-6}$	$5 \cdot 10^{-4}$	$[8.33 \cdot 10^{-6}; 1.034 \cdot 10^{-3}]$	[52,53]	$\frac{mm^3}{mol \cdot min}$
k_{eg}	$9.9256 \cdot 10^{-7}$	$1.1476 \cdot 10^{-6}$	–	–	$\frac{mm^3}{cell}$
k_{ed}	$9.9256 \cdot 10^{-7}$	$8.1969 \cdot 10^{-10}$	–	–	$\frac{mm^3}{cell}$
n^*	$3.0225 \cdot 10^5$	$6.7098 \cdot 10^4$	–	–	$\frac{mm^3}{mol}$
c_n	0.5	0.5	–	–	$\frac{mm^3}{mol}$
c_{sat}	0.9	0.9	–	–	$\frac{mm^3}{mm^3}$
α	$4 \cdot 10^{-8}$	$4 \cdot 10^{-8}$	–	–	$\frac{mm^3}{cell \cdot min}$

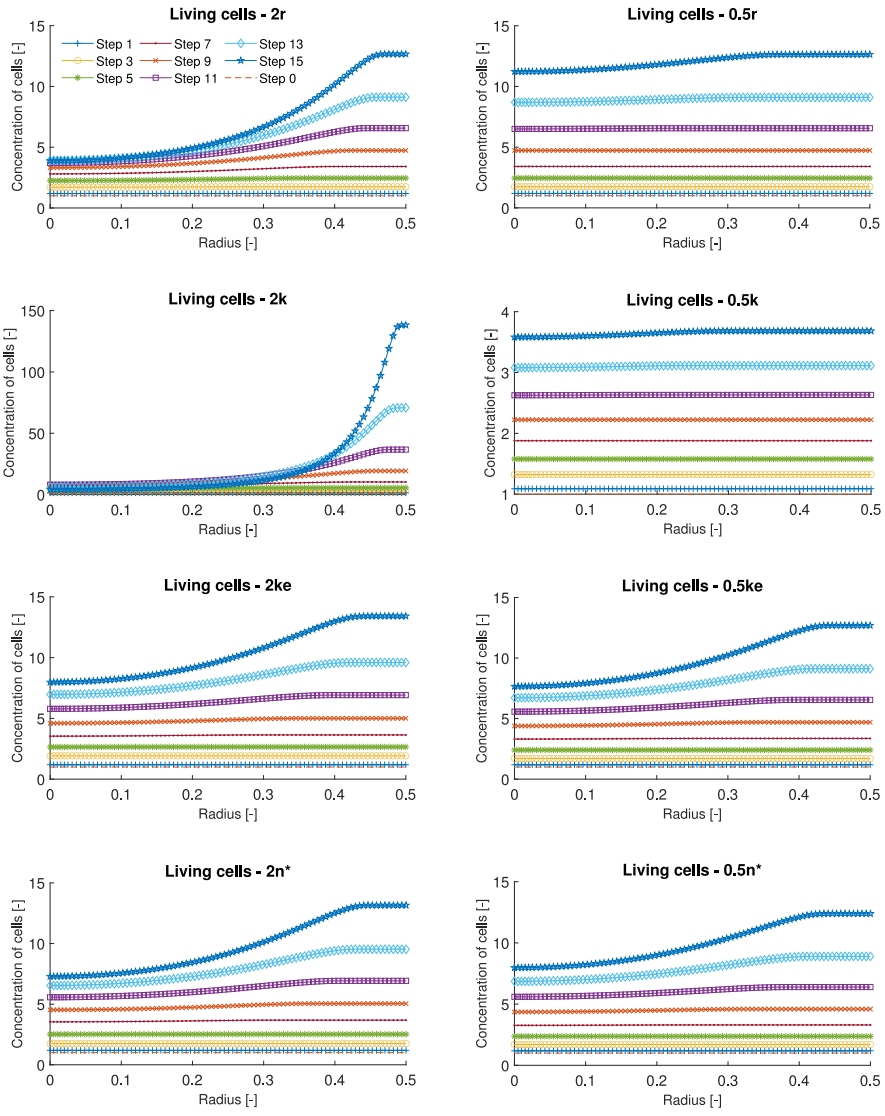

Fig. 4. Parametric analysis of the distribution of the concentration of living cells along the dimensionless radius of the spheroid, at time steps 0, 1, 3, 5, 7, 9, 11, 13 and 15, for cases 2r, 0.5r, 2k, 0.5k, 2ke, 0.5ke, $2n^*$ and $0.5n^*$.

number of hyperelastic models for elastomers and living tissues [58–60]. Hence,

$$\boldsymbol{\varepsilon}^T = \boldsymbol{\varepsilon}^{el} + \boldsymbol{\varepsilon}^{cell} \quad \text{in} \quad \Omega(\mathbf{x}, t) \tag{7}$$

The cell contractility $\boldsymbol{\varepsilon}^{cell}$ is assumed to be isotropically dependent on the activity of cells, and hence on cell concentration n, as follows:

$$\boldsymbol{\varepsilon}^{cell} = k_\varepsilon(n) \cdot n \cdot \mathbf{I} \quad \text{in} \quad \Omega(\mathbf{x}, t) \tag{8}$$

where k_ε is the contractility constant, which depends on the available room for cells to exert contractile forces. Fig. 3 shows a sketch which explains this hypothesis: given an initial state of contraction n_0 [30,37,38] (red circumference with green cells), two different fates can occur, depending on whether the net balance is growth (G) or death (D). In the case of growth, if there is enough room to accommodate more cells, compression (G.I) occurs because the proliferating cells (green plus purple cells) exert contractile forces. When the reference value is overpassed (value of n^* is exceeded), there is no more room for cells and the reference volume expands (G.II and G.III). On the other hand, if the fate is death, cells die by necrosis, and then release their contractile forces producing the expansion of the spheroid (D.I).

The function which models the cell's contractility/expansion, according to the hypothesis above, is shown in Fig. 3. Therefore, the contractility constant k_ε is defined as,

$$k_\varepsilon = \begin{cases} k_{\varepsilon,g} & \text{if } n \geq n^* \\ -k_{\varepsilon,d} & \text{if } n < n^* \end{cases} \tag{9}$$

Several works also consider the shift from compression to expansion. On the one hand, Kopanska et al. [61] studied, from an in vitro point of view, the contractile forces that occur in a spheroid as a consequence of its interaction with the extracellular matrix, concluding that during growth, it undergoes both contraction and expansion as a consequence of its interplay with collagen. On the other hand, Giverso and Preziosi [62] studied the spheroid as a porous material composed of cells and water and established that when it is subjected to radial compression on its surface, it initially undergoes a compressive state with subsequent expansion due to proliferation predominates. In another study, Chen et al. [22], modeled the mechanical interaction between the extracellular matrix and the tumor spheroid, rather than the mechanics among the cells of the spheroid and the tumor spheroid. Mascheroni et al. [19] did not consider a cellular concentration that

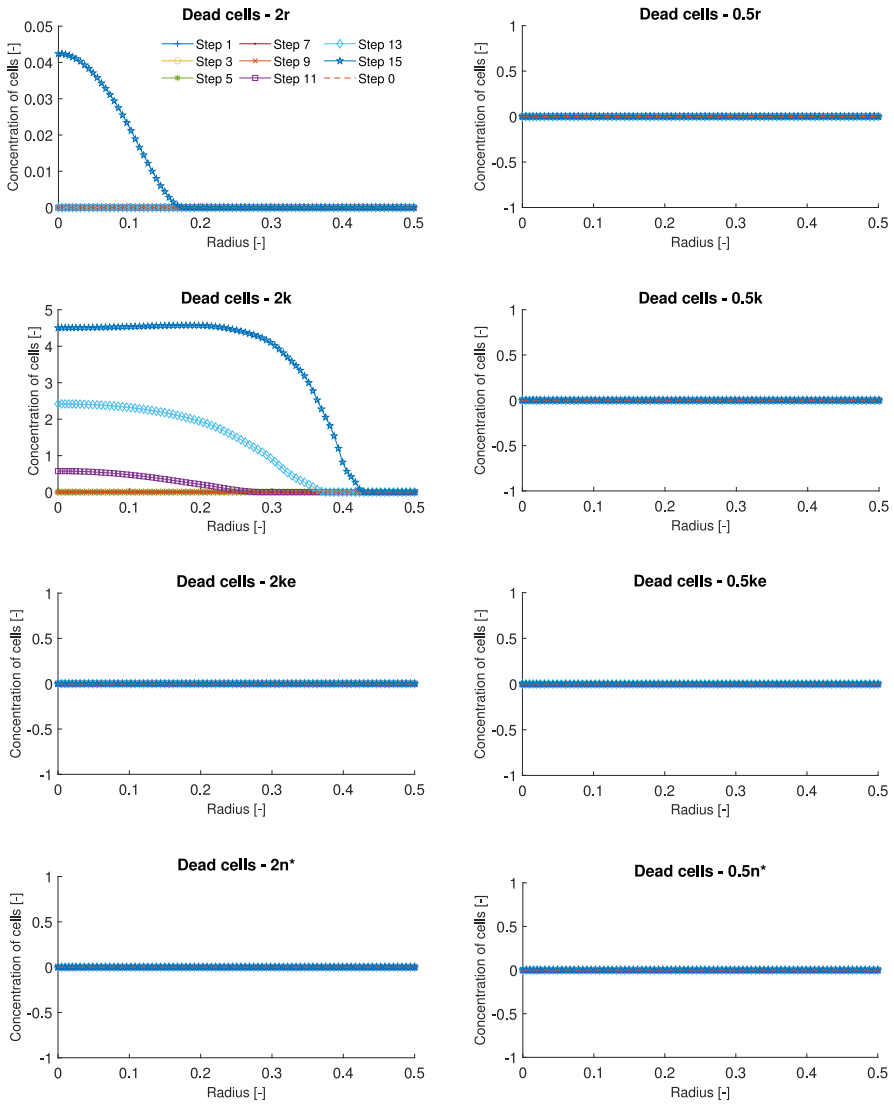

Fig. 5. Parametric analysis of the distribution of the concentration of dead cells along the dimensionless radius of the spheroid, at time steps 0, 1, 3, 5, 7, 9, 11, 13 and 15, for cases 2r, 0.5r, 2k, 0.5k, 2ke, 0.5ke, $2n^*$ and $0.5n^*$.

marks the transition between zones of spheroidal contraction and expansion. In our model the shift from compression to expansion during growth is aligned with the experimental observed behavior, and is regulated by the model parameter n^*.

The remaining equilibrium, compatibility and constitutive equations (linearized for time t around the current configuration $\Omega(\mathbf{x},t)$) read as,

$$\begin{aligned}
&\nabla\cdot\boldsymbol{\sigma}=\mathbf{0}\\
&\boldsymbol{\varepsilon}^T=\tfrac{1}{2}(\nabla\mathbf{u}+\nabla^T\mathbf{u}) \quad \text{in} \quad \Omega(\mathbf{x},t)\\
&\boldsymbol{\sigma}=\mathbf{C}\boldsymbol{\varepsilon}^{el}\\
&\boldsymbol{\sigma}(\mathbf{x},0)=\boldsymbol{\sigma}_0 \quad \text{in} \quad \Omega(\mathbf{x},0)\\
&\mathbf{t}^n(\mathbf{x},t)=\bar{\mathbf{t}}^n \quad \text{in} \quad \Gamma_t(\mathbf{x},t)\\
&\mathbf{u}(\mathbf{x},t)=\bar{\mathbf{u}} \quad \text{in} \quad \Gamma_u(\mathbf{x},t)
\end{aligned} \tag{10}$$

with $\Gamma_b=\Gamma_u\cup\Gamma_t$, $\Gamma_u\cap\Gamma_t=\emptyset$, and $\mathbf{C}$ being the fourth order elasticity tensor which characterizes the mechanical behavior of the spheroid. $\boldsymbol{\sigma}_0$ is a certain initial pre-stress in the spheroid, and $\bar{\mathbf{t}}^n$ and $\bar{\mathbf{u}}$ the prescribed tractions and displacements on the spheroid boundary. These boundary conditions are included in the formulation for completeness purposes, although the analyzed spheroids were considered as free of initial pre-stress, forces and of prescribed displacements along the boundary.

4. Dimensionless formulation

Space and time are now non-dimensionalized as follows:

$$\tilde{\boldsymbol{x}}=\frac{\mathbf{x}}{D_0} \tag{11}$$

$$\tilde{t}=\frac{t}{T_0} \tag{12}$$

with D_0 the diameter of the spheroid, and T_0 a characteristic time of analysis. On the other hand, dimensionless nutrient concentration is defined with reference to the initial concentration of nutrients in the suspension experiment:

$$\tilde{c}(\tilde{\boldsymbol{x}},\tilde{t})=\frac{c(\tilde{\boldsymbol{x}},t)}{c_\Gamma} \tag{13}$$

while the cell concentration is non-dimensionalized versus the initial cell concentration of the spheroid,

$$\tilde{n}(\tilde{\boldsymbol{x}},\tilde{t})=\frac{n(\tilde{\boldsymbol{x}},t)}{n_0} \tag{14}$$

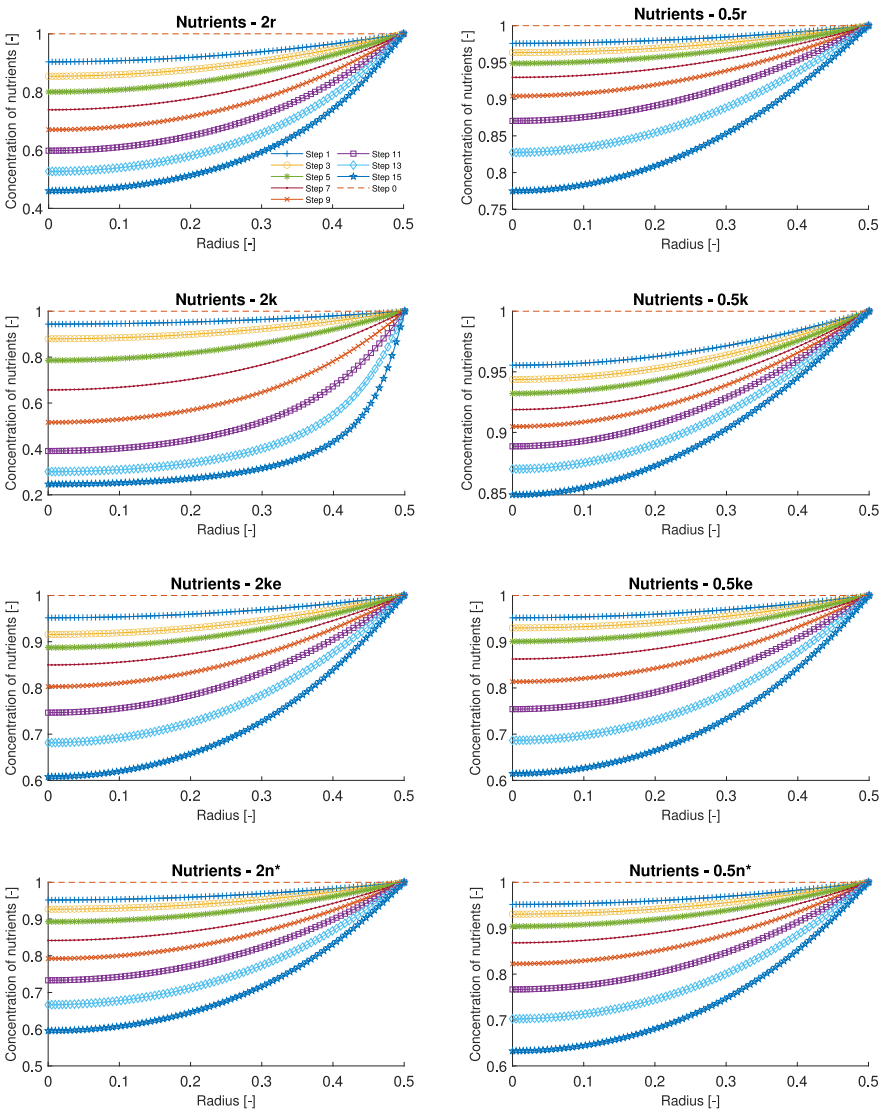

Fig. 6. Parametric analysis of the distribution of the concentration of nutrients along the dimensionless radius of the spheroid, at time steps 0, 1, 3, 5, 7, 9, 11, 13 and 15, for cases 2r, 0.5r, 2k, 0.5k, 2ke, 0.5ke, $2n^*$ and $0.5n^*$.

We assume a linearly elastic isotropic homogeneous constitutive model for the spheroid, defined by two parameters: the elastic modulus (E) and the Poisson's ratio (ν). The stresses are then referred to the elastic modulus of the spheroid:

$$\tilde{\boldsymbol{\sigma}}(\tilde{\boldsymbol{x}},\tilde{t}) = \frac{\boldsymbol{\sigma}(\tilde{\boldsymbol{x}},t)}{E} \tag{15}$$

ν was set to 0.3 in this study.

4.1. Nutrient diffusion

Introducing the dimensionless quantities in Eqs. (11)–(14) in the nutrient diffusion Eq. (1) yields,

$$\begin{aligned}
&\frac{\partial \tilde{c}}{\partial \tilde{t}} = \tilde{k}_c \nabla^2 \tilde{c} - \tilde{r}\cdot\tilde{n} \quad \text{in} \quad \tilde{\Omega}(\tilde{\boldsymbol{x}},\tilde{t})\\
&\tilde{c}(\tilde{\boldsymbol{x}},0) = \tilde{c}_0 \quad \text{in} \quad \tilde{\Omega}(\tilde{\boldsymbol{x}},0)\\
&\tilde{c}(\tilde{\boldsymbol{x}},\tilde{t}) = \tilde{f}(\tilde{\boldsymbol{x}},\tilde{t}) \quad \text{in} \quad \tilde{\Gamma}_b(\tilde{\boldsymbol{x}},\tilde{t})
\end{aligned} \tag{16}$$

with:

$$\begin{aligned}
&\frac{\partial \tilde{f}}{\partial t} = -\tilde{\alpha}\cdot\tilde{n} \quad \text{in} \quad \tilde{\Gamma}_b(\tilde{\boldsymbol{x}},\tilde{t})\\
&\tilde{f}(\tilde{\boldsymbol{x}},0) = 1 \quad \text{in} \quad \tilde{\Gamma}_b(\tilde{\boldsymbol{x}},0)
\end{aligned} \tag{17}$$

where the following dimensionless parameters in Eq. (16) are defined:

$$\begin{aligned}
\tilde{c}_0 &= \frac{c_0}{c_\Gamma}\\
\tilde{k}_c &= \frac{k_c T_0}{D_0^2}\\
\tilde{r} &= \frac{r n_0 T_0}{c_\Gamma}\\
\tilde{\alpha} &= \frac{\alpha n_0 T_0}{c_\Gamma}
\end{aligned} \tag{18}$$

4.2. Cell dynamics

The dimensionless quantities defined in Eqs. (11)–(14) are used in Eqs. (4) and (5), getting,

$$\begin{aligned}
&\frac{\partial \tilde{n}^d}{\partial \tilde{t}} = -\tilde{k}_d\cdot(\tilde{c}_n - \tilde{c})\cdot\tilde{n} \quad \text{if} \quad \tilde{c}\le\tilde{c}_n \quad \text{in} \quad \tilde{\Omega}(\tilde{\boldsymbol{x}},\tilde{t})\\
&\tilde{n}^d(\tilde{\boldsymbol{x}},0) = 0 \quad \text{in} \quad \tilde{\Omega}(\tilde{\boldsymbol{x}},0)
\end{aligned} \tag{19}$$

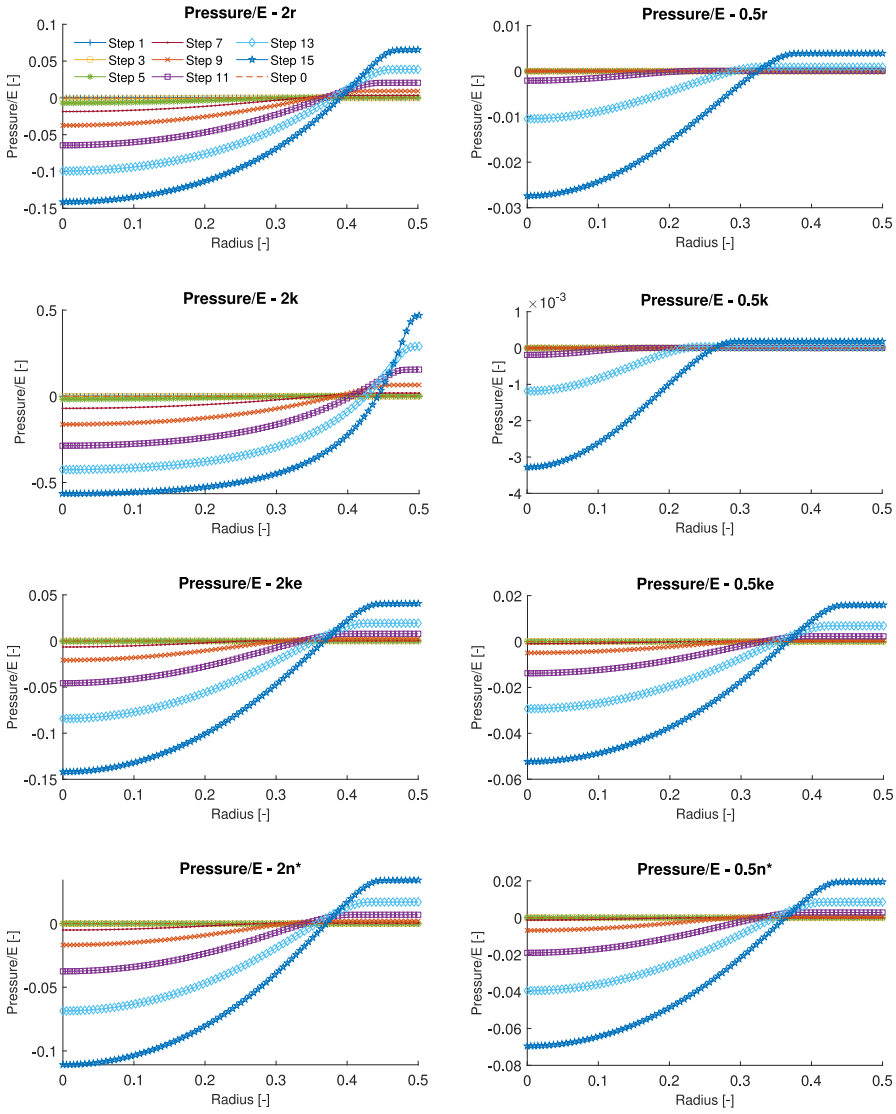

Fig. 7. Parametric analysis of the distribution of pressure along the dimensionless radius of the spheroid, at time steps 0, 1, 3, 5, 7, 9, 11, 13 and 15, for cases 2r, 0.5r, 2k, 0.5k, 2ke, 0.5ke, $2n^*$ and $0.5n^*$.

$$\begin{aligned}
&\frac{\partial \tilde{n}^g}{\partial \tilde{t}} = \tilde{k}_g \cdot (\tilde{c} - \tilde{c}_n) \cdot \tilde{n} \quad \text{if} \quad \tilde{c} > \tilde{c}_n \quad \text{in} \quad \tilde{\Omega}(\tilde{\mathbf{x}}, \tilde{t}) \\
&\frac{\partial \tilde{n}^g}{\partial \tilde{t}} = \tilde{k}_g \cdot (\tilde{c}_{sat} - c_n) \cdot \tilde{n} \quad \text{if} \quad \tilde{c} > \tilde{c}_{sat} \quad \text{in} \quad \tilde{\Omega}(\tilde{\mathbf{x}}, \tilde{t}) \\
&\tilde{n}^g(\tilde{\mathbf{x}}, 0) = 0 \quad \text{in} \quad \tilde{\Omega}(\tilde{\mathbf{x}}, 0)
\end{aligned} \tag{20}$$

$$\tilde{n}(\tilde{\mathbf{x}}, \tilde{t}) = 1 + \tilde{n}^g(\tilde{\mathbf{x}}, \tilde{t}) + \tilde{n}^d(\tilde{\mathbf{x}}, \tilde{t}) \tag{21}$$

appearing the following dimensionless parameters in Eqs. (19) and (20):

$$\begin{aligned}
\tilde{k}_d &= \frac{k_d T_0}{n_0 c_\Gamma} \\
\tilde{k}_g &= \frac{k_g T_0}{n_0 c_\Gamma} \\
\tilde{c}_n &= \frac{c_n}{c_\Gamma} \\
\tilde{c}_{sat} &= \frac{c_{sat}}{c_\Gamma}
\end{aligned} \tag{22}$$

Now, taking the time derivative of Eq. (21) yields,

$$\frac{\partial \tilde{n}}{\partial \tilde{t}} = \frac{\partial \tilde{n}^g}{\partial \tilde{t}} + \frac{\partial \tilde{n}^d}{\partial \tilde{t}} \tag{23}$$

Considering Eqs. (19) and (20), Eq. (23) may be rewritten as:

$$\begin{aligned}
&\frac{\partial \tilde{n}}{\partial \tilde{t}} = -\tilde{k}_d \cdot (\tilde{c}_n - \tilde{c}) \cdot \tilde{n} \cdot \delta_1 + \tilde{k}_g \cdot (\tilde{c} - \tilde{c}_n) \cdot \tilde{n} \cdot \delta_2 \\
&\quad + \tilde{k}_g \cdot (\tilde{c}_{sat} - c_n) \cdot \tilde{n} \cdot \delta_3 \quad \text{in} \quad \tilde{\Omega}(\tilde{\mathbf{x}}, \tilde{t}) \\
&\tilde{n}(\tilde{\mathbf{x}}, 0) = 1 \quad \text{in} \quad \tilde{\Omega}(\tilde{\mathbf{x}}, 0)
\end{aligned} \tag{24}$$

with,

$$\begin{cases}
\delta_1 = 1 \quad \text{if} \quad \tilde{c} \leq \tilde{c}_n \quad \text{and} \quad \delta_1 = 0 \quad \text{elsewhere} \\
\delta_2 = 1 \quad \text{if} \quad \tilde{c}_n < \tilde{c} \leq \tilde{c}_{sat} \quad \text{and} \quad \delta_2 = 0 \quad \text{elsewhere} \\
\delta_3 = 1 \quad \text{if} \quad \tilde{c} > \tilde{c}_{sat} \quad \text{and} \quad \delta_3 = 0 \quad \text{elsewhere}
\end{cases} \tag{25}$$

Eq. (24) will be used to compute the cell evolution in the spheroid. Dead and alive cells can be computed afterwards from Eqs. (19) and (20).

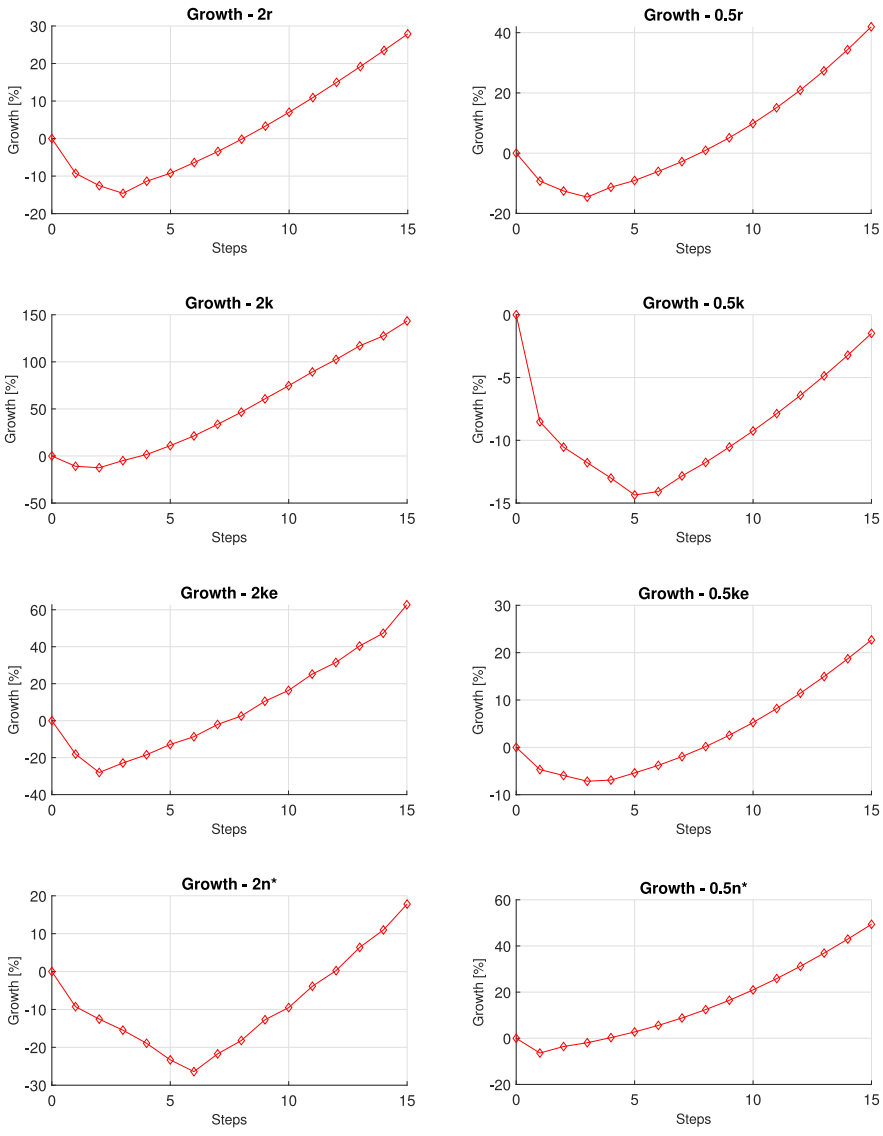

Fig. 8. Parametric analysis of the evolution of the spheroid section from the initial step to the 15th, for the cases 2r, 0.5r, 2k, 0.5k, 2ke, 0.5ke, $2n^*$ and $0.5n^*$.

4.3. Cell mechanics

For the cell mechanics equations, we introduce the dimensionless quantities in Eqs. (11), (12) and (14) in Eq. (8), getting:

$$\boldsymbol{\epsilon}^{cell} = \tilde{k}_{\epsilon} \cdot \tilde{n} \cdot \mathbf{I} \quad \text{in} \quad \tilde{\Omega}(\tilde{\boldsymbol{x}}, \tilde{t}) \tag{26}$$

with,

$$\tilde{k}_{\epsilon} = \begin{cases} \tilde{k}_{\epsilon,g} & \text{if } \tilde{n} \geq \tilde{n}^* \\ -\tilde{k}_{\epsilon,d} & \text{if } \tilde{n} < \tilde{n}^* \end{cases} \tag{27}$$

Using again the dimensionless quantities in Eqs. (11), (12) and (15) in Eq. (10), we obtain:

$$\begin{aligned} &\nabla \cdot \tilde{\boldsymbol{\sigma}} = \mathbf{0} \\ &\boldsymbol{\epsilon}^T = \tfrac{1}{2}(\nabla \tilde{\mathbf{u}} + \nabla^T \tilde{\mathbf{u}}) \quad \text{in} \quad \tilde{\Omega}(\tilde{\boldsymbol{x}}, \tilde{t}) \\ &\tilde{\boldsymbol{\sigma}} = \tilde{\mathbf{C}} \boldsymbol{\epsilon}^{el} \end{aligned} \tag{28}$$

The following dimensionless parameters in Eqs. (26)–(28) are then defined:

$$\begin{aligned} &\tilde{\boldsymbol{u}}(\tilde{\boldsymbol{x}}, \tilde{t}) = \frac{\mathbf{u}(\tilde{\boldsymbol{x}}, \tilde{t})}{D_0} \\ &\tilde{\boldsymbol{k}}_{\boldsymbol{\epsilon}} = \boldsymbol{k}_{\boldsymbol{\epsilon}} n_0 \\ &\tilde{n}^* = \frac{n^*}{n_0} \\ &\tilde{\boldsymbol{C}} = \frac{\boldsymbol{C}}{E} \end{aligned} \tag{29}$$

5. Numerical implementation

The multiphysics coupled model described above is composed of the nutrient diffusion Eq. (16), cell dynamics evolution Eq. (24) and cell mechanics Eqs. (7), (26) and (28). These equations are numerically implemented following an updated Lagrangian scheme. Therefore, the governing equations of the model are solved at each j-step at time t_j for the updated configuration $\tilde{\boldsymbol{x}}_j$ as described in Box 1.

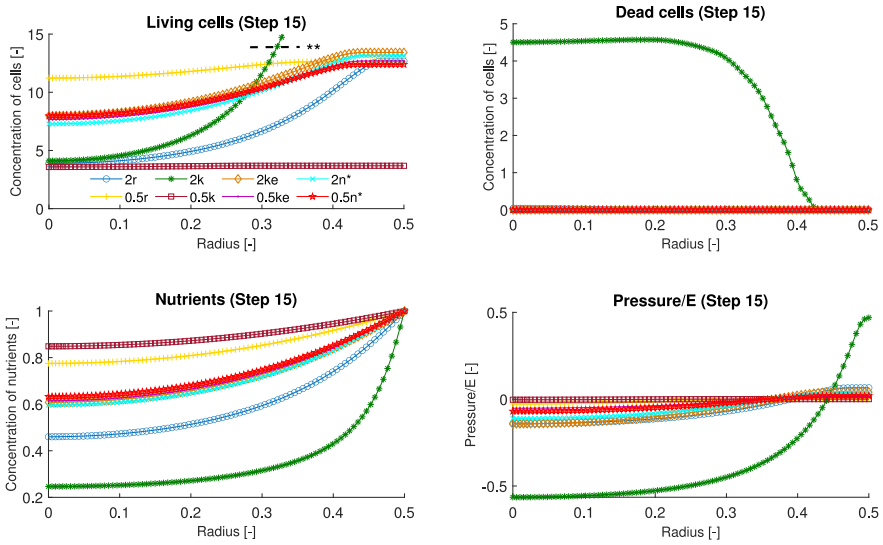

Fig. 9. Values of the analyzed quantities in the parametric analysis at the final step, for the different variations of parameters 2r, 0.5r, 2k, 0.5k, 2ke, 0.5ke, $2n^*$ and $0.5n^*$. In the upper left graph, ** means that the value of the concentration of living cells at radius 0.5 [-], for 2k, is 138.23.

Box 1: Multiphysics model implementation scheme.

1. Set j-step $j = 0$.
   Initialize initial configuration $\tilde{\boldsymbol{x}}_j = \tilde{\boldsymbol{x}}_0$, initial time of analysis $\tilde{t}_j = \tilde{t}_0$ and time increment $\Delta\tilde{t}$.
   Initialize field variables:
   $$\begin{aligned} \tilde{c}_j &= \tilde{c}_0 \\ \tilde{n}_j &= 1 \\ \tilde{\mathbf{u}}_j &= \mathbf{0} \end{aligned} \tag{30}$$
   For $j = 1..Nsteps$
2. Solve:
   $$\begin{aligned} \tilde{c}_{j+1} &= \tilde{c}_j + (\tilde{k}_c \nabla^2 \tilde{c}_{j+1} - \tilde{r}\tilde{n}_{j+1}) \cdot \Delta\tilde{t} \quad \text{in} \quad \tilde{\Omega}(\tilde{\boldsymbol{x}}_j) \\ \tilde{c}_{j+1} &= \tilde{f}_j - \tilde{\alpha} \cdot \tilde{n}_j \cdot \Delta\tilde{t} \quad \text{in} \quad \tilde{\Gamma}(\tilde{\boldsymbol{x}}_j) \\ \tilde{n}_{j+1} &= \tilde{n}_j + [-\tilde{k}_d \cdot (\tilde{c}_n - \tilde{c}_{j+1}) \cdot \tilde{n}_{j+1} \cdot \delta_1 + \\ &+\tilde{k}_g \cdot (\tilde{c}_{j+1} - \tilde{c}_n) \cdot \tilde{n}_{j+1} \cdot \delta_2 + \tilde{k}_g \cdot (\tilde{c}_{sat} - \tilde{c}_n) \cdot \tilde{n}_{j+1} \cdot \delta_3] \cdot \Delta\tilde{t} \\ &+\text{initial and boundary conditions} \end{aligned} \tag{31}$$
3. Given $\tilde{n}_{j+1}$, solve:
   $$\begin{aligned} \nabla \cdot \tilde{\boldsymbol{\sigma}}_{j+1} &= \mathbf{0} \\ \tilde{\boldsymbol{\sigma}}_{j+1} &= \tilde{\mathbf{C}}\boldsymbol{\epsilon}^{el}_{j+1} \\ \boldsymbol{\epsilon}^{cell}_{j+1} &= \tilde{k}_\epsilon \cdot \tilde{n}_{j+1} \cdot \mathbf{I} \quad \text{in} \quad \tilde{\Omega}(\tilde{\boldsymbol{x}}_j) \\ \boldsymbol{\epsilon}^{T}_{j+1} &= \boldsymbol{\epsilon}^{el}_{j+1} + \boldsymbol{\epsilon}^{cell}_{j+1} \\ \boldsymbol{\epsilon}^{T}_{j+1} &= \tfrac{1}{2}(\nabla\tilde{\mathbf{u}}_{j+1} + \nabla^T\tilde{\mathbf{u}})_{j+1} \\ &+\text{initial and boundary conditions} \end{aligned} \tag{32}$$
4. Set:
   $\tilde{\boldsymbol{x}}_{j+1} = \tilde{\boldsymbol{x}}_j + \tilde{\mathbf{u}}_{j+1}$
   $\tilde{t}_{j+1} = \tilde{t}_j + \Delta\tilde{t}$
5. Update concentrations to new configurations:
   $\tilde{c}_{j+1} \leftarrow \tilde{c}_{j+1} \cdot |\mathbf{F}^{-1}_{j+1}|$
   $\tilde{n}_{j+1} \leftarrow \tilde{n}_{j+1} \cdot |\mathbf{F}^{-1}_{j+1}|$
6. Set $j \leftarrow j + 1$:
7. GOTO 2.
   End For

First, after initialization of the field variables and initial domain, a backward-Euler scheme is followed to discretize in time the nutrient diffusion and the cell dynamics equations. These equations are solved together (strongly coupled) according to Eq. (31) in Box 1. Then, the cell mechanics equations (Eq. (32)) are solved. Notice that these equations are weakly coupled with the nutrient diffusion and cell dynamics, for a given cell concentration $\tilde{n}_{j+1}$. Then, the new deformed configuration is updated, and both nutrient and cell concentrations are updated through the deformation gradient $\mathbf{F}_{j+1}$ of the solution (see item 5 in box 1). This process is iteratively repeated until the end of the analysis is reached (see Box 1).

Eqs. (31) and (32) are spatially discretized following a finite element (FE) numerical framework. Thus, these Eqs. are firstly written in their weak form (the reader is referred to Zienkiewicz and Taylor [63] for the basics of FE analysis). Then, the field variables in Eqs. (31) and (32) are approximated as follows:

$$\begin{aligned} \tilde{c}_{j+1}(\tilde{\boldsymbol{x}}_j) &= \mathbf{N}_{\tilde{c}}(\tilde{\boldsymbol{x}}_j) \cdot \tilde{\mathbf{C}}_{j+1} \\ \tilde{n}_{j+1}(\tilde{\boldsymbol{x}}_j) &= \mathbf{N}_{\tilde{n}}(\tilde{\boldsymbol{x}}_j) \cdot \tilde{\mathbf{N}}_{j+1} \\ \tilde{\mathbf{u}}_{j+1}(\tilde{\boldsymbol{x}}_j) &= \mathbf{N}_{\tilde{\mathbf{u}}}(\tilde{\boldsymbol{x}}_j) \cdot \tilde{\mathbf{U}}_{j+1} \end{aligned} \tag{33}$$

where $\mathbf{N}_{\tilde{c}}$, $\mathbf{N}_{\tilde{n}}$ and $\mathbf{N}_{\tilde{\mathbf{u}}}$ are shape function (interpolating) matrices for the continuum variables $\tilde{c}$, $\tilde{n}$ and $\tilde{\mathbf{u}}$, respectively. On the other hand, $\tilde{\mathbf{C}}_{j+1}$, $\tilde{\mathbf{N}}_{j+1}$ and $\tilde{\mathbf{U}}_{j+1}$ are noded-value vectors at the nodal positions of the FE mesh for nutrient concentration, cell concentration and spheroid displacements, respectively, at the current configuration $\tilde{\boldsymbol{x}}_j$.

Eqs. (31) and (32) are implemented using the commercial FE software Abaqus Simulia. First, Eq. (31) are solved as a Heat Transfer analysis, where the source term is implemented in Abaqus by means of the `HETVAL` subroutine. Moreover, the cell dynamics evolution is also implemented in this subroutine. On the other hand, Eq. (32) is solved using a static solid mechanics analysis in Abaqus. In this context, the term ϵ^{cell} is imposed analogously to a temperature in a thermal–mechanical problem. The whole scheme in Box 1 is orchestrated by Matlab R2017a in an in-house main code. The input and output data needed for the different computations in Box 1, are exchanged via writing and reading files along the Matlab and Abaqus subroutines (`URDFIL`).

6. Results

6.1. Parametric analysis

In order to investigate the influence of the different model parameters on the evolution of the field variables and results, the dimensionless model shown in the previous sections was repeatedly run for a set of parameters. Therefore, we vary up to 4 parameters from their reference value as shown in Table 3. The reference values for first four parameters

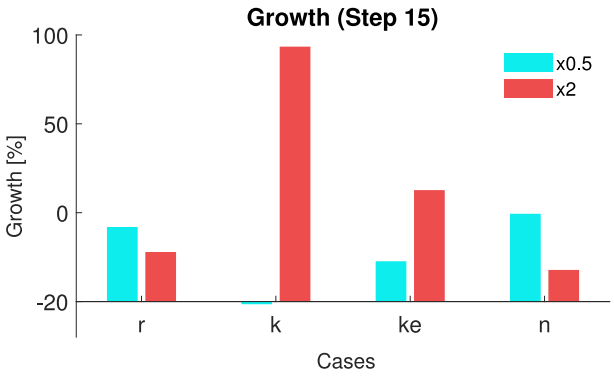

Fig. 10. Spheroid growth at the final step of the parametric analysis, for the different variations of parameters 2r, 0.5r, 2k, 0.5k, 2ke, 0.5ke, $2n^*$ and $0.5n^*$.

shown in Table 3 were taken from the literature [39,48–53] from models of glioblastoma multiforme cell lines and related brain tumors, as shown in Table 4, but in dimensionless units. The rest of parameters were specifically introduced in our model, so the corresponding reference values were chosen from the order of magnitude of the calibrated parameters during validation (see Section 3.2), but in dimensionless units. From the parameters shown in Table 3, we decided to vary a subset of them. $\tilde{k_c}$ was excluded from the parametric analysis as it showed a minor impact on the results in preliminary simulations. On the other hand, $\tilde{c}_n$ and $\tilde{c}_{sat}$ were excluded from the parametric analysis and fixed to 0.5 and 0.9 since they represent intermediate and high levels (in the range 0–1), of nutrient concentration, respectively, according to their definition in Section 3.2. The selected parameters have a clear physiological relevance such as nutrient consumption of cells ($\tilde{r}$), kinetics of cell death and growth ($\tilde{k}_d$ and $\tilde{k}_g$, respectively); and cell compression and expansion constants ($\tilde{k}_{ed}$ and $\tilde{k}_{eg}$, respectively). From the reference value of the parameters, the variation was set for all cases from half to double the reference value (see Table 3). Since $\tilde{k}_d - \tilde{k}_g$ and $\tilde{k}_{ed} - \tilde{k}_{eg}$ are varied at the same ratio, they are referred as $\tilde{k}$ and $\tilde{k}_e$, respectively.

We considered a uniform dimensionless nutrient concentration equal to 1 on the spheroid boundary for all the analysis time interval, and within the spheroid at the initial time of analysis. Moreover, we considered an initial cell concentration equal to 1, and null concentration of dead cells. Finally, the spheroid was free of body forces at the initial time of analysis and free of boundary forces/movements along the whole time period of analysis to simulate the suspension conditions of the spheroids in the experiments. The domain of the spheroid was modeled using 3D finite elements. In particular, the unit (dimensionless) sphere was discretized with 49000 hexahedra and 49491 nodes. Even though the model has circumferential symmetry, we modeled the full sphere for an easier visualization of the results. The time increment (step) used in the simulations was set to 1/12. It was checked that the selected mesh and time step showed results independency and convergence.

The evolutions of living cell concentration, dead cell concentration, nutrient concentration and pressure (i.e. one third of the first invariant of the stress tensor) are shown in Figs. 4–7 along the radius of the spheroid for different time steps. Furthermore, the growth of the spheroid is computed as the (percentage) of the projected area of the spheroid referred to the initial configuration, whose evolution is plot in Fig. 8. Finally, Figs. 9 and 10 shows the evolution of the variables at step 15, for the different parameter combinations.

6.2. Validation results

In this section, we validate the proposed mechanobiological model with the experimental results obtained in the tests described in Section 2. The calibration of model parameters was established as follows. The model parameters of our model that are present or similar to other models were estimated from the literature as indicated in Table 4. Other parameters of our model that appears from the proposed laws of our model (Figs. 2 and 3) were fitted using a trial and error procedure given the complexity of our coupled modeling. However, the fitting was accelerated from the understanding of model parameters on results, conducted in Section 3.1. We checked that validation was possible for a unique set of values of model parameters within the bibliographic range.

The evolution of a spheroid composed of U-87 glioblastoma cell line is shown in Fig. 11, for different times of the analysis. These results are plot in terms of the percentage of projected area in Fig. 12 for the different spheroids in the experiment. Moreover, the corresponding result of the model is also included in Fig. 12 for comparison purposes. The model was run for a time step of 120 min during a simulation time interval of 14 days (168 steps). The results presented in Figs. 12 and 15 correspond to time points analogous to the experimental ones. According to the experimental data, there is an initial growth of the spheroid volume that stabilizes over time. In this period, the spheroid increases in size almost six times. A good agreement can be found between the model results and the evolution of the different spheroids. The evolution of the model variables is shown in Fig. 13. Living and dead cell concentrations (and associated model parameters) are shown as dimensional quantities. However, the nutrient concentration and stress (and associated model parameters) were referred to their dimensionless values.

On the other hand, the evolution of a different glioblastoma cell line, U-251, is shown for a spheroid in Fig. 14. These results are compared for differed spheroids versus the model outcome in Fig. 15. In this case, the model was calibrated for a different set of parameters, as seen in Table 4, since they are referred to different cells and behavior. Using this calibration, we can see in Fig. 15 that the curve of the model lies within the experimental range and according to the experimental data of the different spheroids in the test. In these assays, the spheroid (on average) reduces its size by almost half in the days of study. Finally, the evolution of model variables is shown in Fig. 16.

7. Discussion

In this paper, we propose a multiphysics mechanobiological model to simulate the evolution of tumor spheroids. Our mechanobiological model includes, in a coupled way, nutrient diffusion, nutrient concentration-dependent cell proliferation/death and cell mechanics as a function of cell concentration. Indeed, the model outcomes were qualitatively validated with our own experiments for glioblastoma spheroids. Previous existing papers in the literature do not consider all these features in the same study. For example, some models do not consider nutrient diffusion [19,26], whereas others do not model cell proliferation [23]. On the other hand, some studies are just validated against experimental data taken from the literature [18,25], or the application is not shown for spheroids [20]. This mixed in silico/experimental approach uniquely combines all the above-mentioned features in the same study. The biological assumptions of the spheroidal model here developed are mainly two: (i) cell dynamics depend on nutrient concentration and (ii) volume variation of the spheroid is related to cell contractility and concentration. With respect to the first one, it was verified to some extent in our experiments (data not shown) in which nutrient recharging/refreshing affected the growth rate of the U-87 cell line (more proliferative line). With respect to the second hypothesis, only the net volume variation can be indirectly evaluated by monitoring the area of the spheroid. We consider this statement as an assumption, based on previous studies in the literature [30,37,38,61,62]. As a result, our model predicts a higher proliferation rate for abundant levels of nutrients, and cell death/dormancy for low levels of nutrients. This behavior is aligned with other models and observed

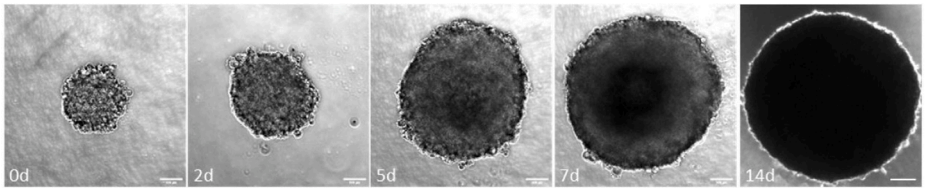

Fig. 11. Experimental images of the evolution of the spheroid on days 0, 2, 5, 7 and 14, for the U-87 cell line. The scale bar is 100 μm.

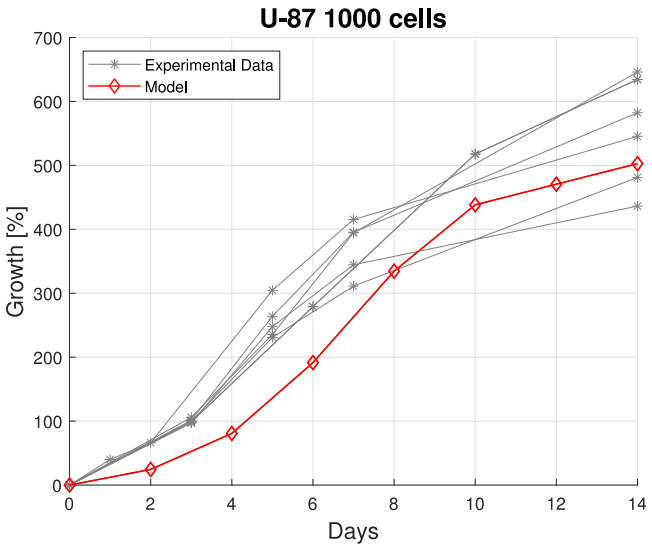

Fig. 12. Evolution of the spheroid projected area over time for the U-87 cell line.

experimental behaviors [30]. Moreover, a material point exerts a high contractility and contractile force, according to our model, for high concentration of cells if there is room enough to accommodate the new cell population. On the other hand, our model predicts an expansion of the volume if cells grow and fill the volume of reference and therefore accommodate to a new expanded volume (see Fig. 3). This hypothesis is similar to the behavior observed in agent-based models [27,29]: in these models cells are considered as (discrete) contractile elements which evolves until a (contracted or expanded) equilibrium state that accommodates the new daughter cells. This behavior is also aligned with experimental evidences [37,38].

The developed mechanobiological model contains a number of phenomenological parameters with physiological meaning. In fact, these parameters may be measured (or calibrated) using standard experiments of proliferation, diffusion [16], or traction force microscopy [64,65] to account for the contractile behavior of glioblastoma cells. The effect of model parameters on the results was investigated in a parametric analysis, using the same rate of variation (from half to double) for all the parameters. It can be seen that contractility constants $\tilde{k}_e$ and $\tilde{n}^*$ have a minor effect on the living cells concentration according to Fig. 4. However, kinetics of cell growth/death constants have a great influence on the cell concentration evolution, with values ranging from 150 to 4 times the initial concentration in the periphery of the spheroid at the end of the analysis. On the other hand, the nutrient consumption constant has an influence on the distribution of living cells within the spheroid, with lower cells at the interior for high consumption rates due to limited availability of nutrients in this place. What is more, the parametric study shows that dead cells only appear in the cases of high nutrient consumption rates and a high rate of dead cells, as expected. In these situations, dead cells rise predominantly in the interior of the spheroid at the last steps of the analysis (see Fig. 5). As seen in Fig. 6, the most influential parameters on nutrient diffusion are the nutrient consumption and kinetics of cell death/growth constants. Specifically, there is more availability of nutrients for low values of nutrient consumption and a low kinetics of cells (low cells concentration). Finally, it can be observed in Fig. 7 that the outer part of the spheroid is under tension and the interior part under compression. Also, the highest pressures appear (either tension or compression) for the most proliferative (higher kinetic constant) cells. Note that the lower kinetic constant case shows the lowest pressure distribution (of the order of 10^{-3}). This case exhibits a monotonically decreasing (negative) growth, Fig. 8, due to the low concentration of cells (see Fig. 4) along time.

The trend of the evolution of the spheroid area is similar for all the analyzed cases (see Fig. 8): there is an initial decay in the first steps (sooner or later depending on the parameters), followed by an increasing growth trend until the end of the analysis. The highest spheroid growth at the end of the analysis appears for the higher kinetic constant (up to 150%), followed by the cases of higher contractile/expansion constant $\tilde{k}_e$ and lower $\tilde{n}^*$ (volume availability or spheroid compaction at the initial step). The highest spheroid contraction in the first steps of the analysis is produced for higher contractile/expansion constant $\tilde{k}_e$ and high $\tilde{n}^*$. It is also interesting to remark that the minimum of growth decay (spheroid compression) is reached faster for higher growth kinetics and lower $\tilde{n}^*$. Note that all the influence of model parameters and observed trends in Figs. 4–8 are aligned with the meaning and definition of these parameters, making sense of the obtained results although it cannot be interpreted as an experimental validation of the model.

However, the proposed mechanobiological model is qualitatively validated for different glioblastoma tumor cells, namely U-87 and U-251 cell lines. In the experiments, spheroid formation starts with the cell suspension and the accumulation of cells at the tip of the hanging drop due to gravity. As the cells cannot attach to any surface, they can only aggregate in a process driven by intercellular connections. This promotes the formation of quasi-spherical structures by the contraction of the starting aggregates. This initial formation process was not experimentally quantified in this study since it is challenging to visualize the cells within the hanging drop because of the large focal distance. However, it has been explained in the literature that spheroid formation consists of three main phases: initial aggregation of isolated cells, followed by spheroid compaction (shrinking), and spheroid growth [66–68]. The duration of the compaction and shrinking phases is cell-type dependent [68,69] and is promoted by intercellular adhesion forces [70,71]. Later, once the quasi-spherical structures are formed, the cells start to proliferate. As mentioned above, the pressure is higher in highly proliferative cells, so it can exceed the adhesion forces between cells and lead to the spheroid size increase. The model outcomes presented in Figs. 12 and 15, were obtained after calibration of the model parameters as shown in Table 4. We maintained the reference values of k_c, c_n and c_{sat}, while we calibrated the consumption of nutrients, proliferative capacity or contractile behavior for the different analyzed cell lines since they are related to specific characteristic and physiology of the cell.

A tumor spheroid is a structure consisting of different layers. The outermost layer receives more nutrients and oxygen from the medium, therefore, it is composed of proliferating living cells [27,72,73]. As one moves inward, the cells find it more difficult to receive nutrients and oxygen [27,72]. For this reason, the center of the spheroid is composed mainly of dead cells. In the case of the U-87 MG cell line, the cells

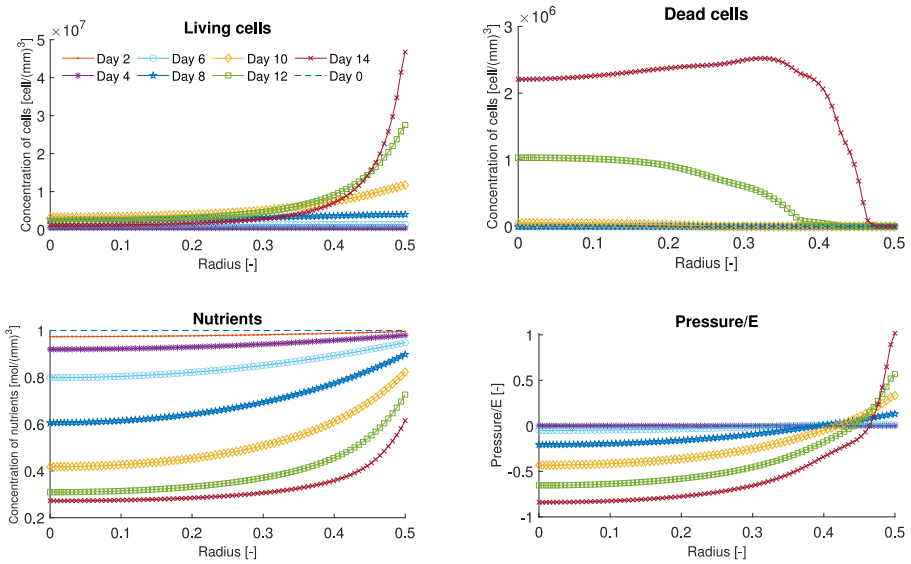

Fig. 13. Distribution of the concentration of living and dead cells, nutrients and pressure along the dimensionless radius of the spheroid, on days 2, 4, 6, 8, 10, 12 and 14, for the U-87 cell line.

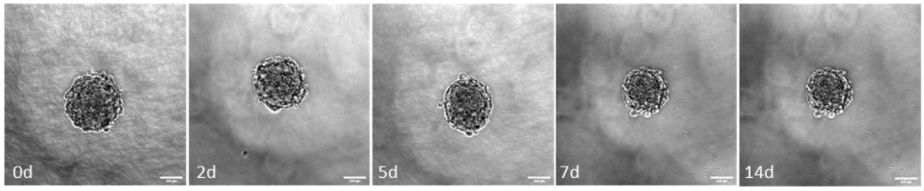

Fig. 14. Experimental images of the evolution of the spheroid on days 0, 2, 5, 7 and 14, for the U-251 cell line. The scale bar is 100 μm.

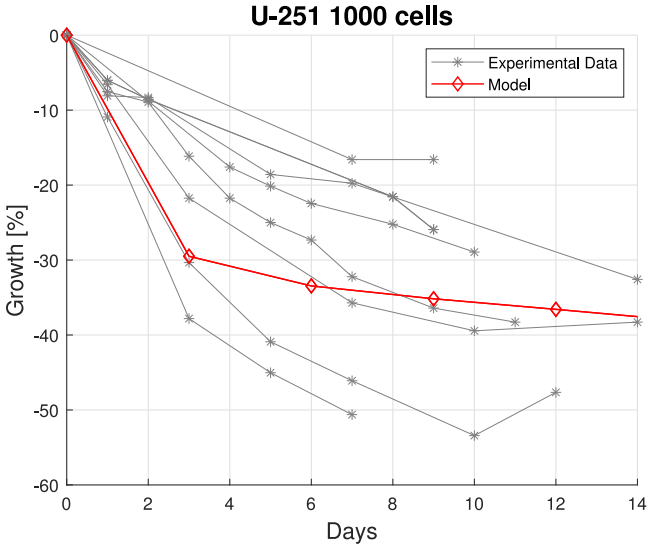

Fig. 15. Evolution of the spheroid projected area over time for the U-251 cell line.

are more proliferative with a higher rate of nutrient consumption [74]. Therefore, the daughter cells, located in the proliferative layer, the outermost layer, originate traction in this area, which in turn causes more accumulation of dead cells in the innermost layer, leaving the necrotic layer in a state of compression [27]. This observed behavior is qualitatively reproduced by our model, as shown in Fig. 13. Interestingly, the fitted parameters for U-251 cell line resulted into flat gradients of nutrients, and consequently a more homogeneous cell distribution and absence of pressure along the spheroid (see Fig. 16). Differences between these cell lines were already studied and it was shown that U-251 cells can survive better in conditions of low nutrient and oxygen concentrations [74]. In our experiments, U-251 spheroids were small and continued reducing their size over time, reaching around 200 μm diameter in 14 days. These cells barely proliferated in 3D culture, so we suspect that strong intercellular interactions were responsible for that size reduction. Meanwhile, U-87 cells were highly proliferative, so the spheroids grew and the diameter of U-87 spheroids reached 800 μm in 14 days. It was observed in tissues that oxygen can reach cells that are 100-200 μm away from blood vessel [47]. This was confirmed in spheroids, as gradients of oxygen and nutrients, and consequent formation of necrotic core depend on the spheroid size. Spheroids whose diameter was bigger than 500 μm developed physicochemical gradients sufficient to induce necrotic core formation [9]. Different cellular behavior, diffusion distances reported in literature [9,47] and spheroid sizes obtained in our experiments can explain our fitted parameters. As U-251 spheroids were small, the model predicted that all cells could get enough oxygen and nutrients, and, as these cells did not proliferate much in the spheroid culture, gradients did not change during the experiment (see Fig. 16). On the other hand, U-87 proliferative cells increased spheroid size, so gradients of oxygen and nutrients were formed as seen in Fig. 13. Cells in the interior of the spheroid did not get components necessary for survival, so cell death was activated and necrotic core was formed (Fig. 13). The distribution of nutrients in the spheroid and formation of gradients for this case can be seen in Fig. 17. In any case, fitted parameters rely within the order of magnitude of different models and simulations available in the literature, according to Table 4.

8. Conclusions

We have proposed a continuum mechanobiological model to study the evolution of spheroids. The model includes the main fundamental

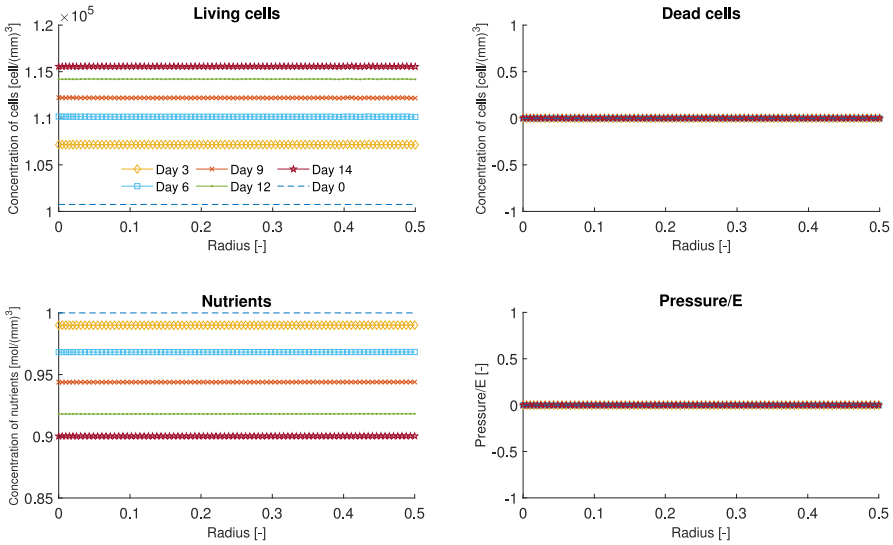

Fig. 16. Distribution of the concentration of living and dead cells, nutrients and pressure along the dimensionless radius of the spheroid, on days 3, 6, 9, 12, and 14, for the U-251 cell line.

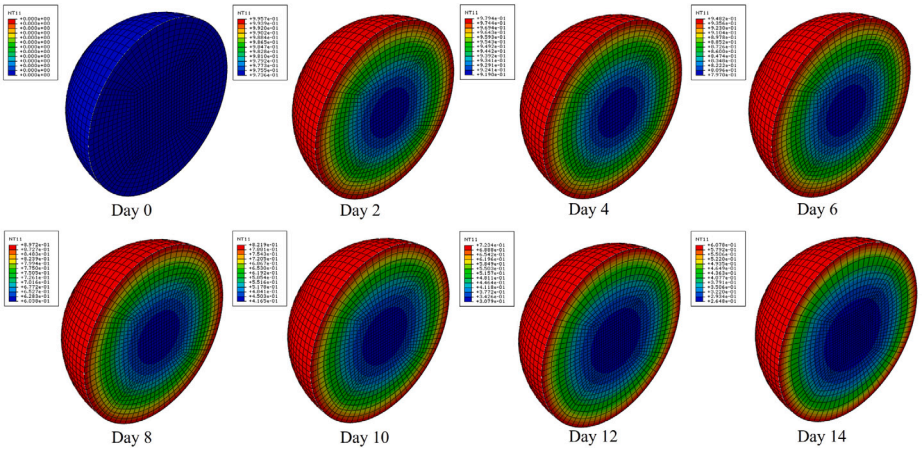

Fig. 17. Distribution of nutrient concentration [-] within the spheroid (half cut).

processes in these applications, namely, diffusion of nutrients, dynamics of cell growth/death, and mechanical interactions among cells. Spheroid cross section evolution predicted by the model was qualitatively validated versus some experiments composed with glioblastoma tumor spheroids that were designed and performed in this work. Different tumoral, U-87 and U-251 cell lines were studied, and the trends (in terms of volume change evolution) were properly captured by the model after calibration of the physiological parameters. In particular, our model is able to capture, in an approximate way, quite different spheroid evolutions, such as growth (up to six times the initial configuration for U-87 cell line) or shrinking (almost half of the initial configuration for U-251 cell line). The main original contribution of this work is deriving the spheroid evolution from the mechanical activity of cells, coupled with nutrient consumption and the subsequent cell dynamics. This model can be used to further investigate mechanistic effects at different observation scales in the evolution of tumors and their role in cancer disease by means of the design of in vitro and/or in silico tests. However, a limitation of our work is that some variables and quantities of our model cannot be explicitly compared and validated with the available experimental outcomes. Quantifying some of these magnitudes, such as the cellular concentration of live and dead cells in different regions of the interior of the spheroid, will be explored as part of our future work. On the other hand, measuring internal pressure within the spheroid would require complex experimental setups to get reliable data. In this context, our proposed model may be used, after additional validation, as a complementary tool to obtain quantities and information in silico, that may be hardly experimentally measured due to technical limitations.

Declaration of competing interest

The authors declare that they have no known competing financial interests or personal relationships that could have appeared to influence the work reported in this paper.

Acknowledgments

The authors gratefully acknowledge the financial support from project PGC2018-097257-B-C31 by the Ministerio de Ciencia e Innovación (MCI), Agencia Estatal de Investigación (AEI) and Fondo Europeo de Desarrollo Regional (FEDER). A.C.-M. was supported by grant PRE2019-090391. H.C.-A., T.R., I.O. and M.D. were supported by the Government of Aragon (DGA) and the Centro de Investigación Biomédica en Red en Bioingeniería, Biomateriales y Nanomedicina (CIBER-BBN). CIBER-BBN is financed by the Instituto de Salud Carlos III with assistance from the European Regional Development Fund.

References

[1] Ana S. Nunes, Andreia S. Barros, Elisabete C. Costa, André F. Moreira, Ilídio J. Correia, 3D tumor spheroids as in vitro models to mimic in vivo human solid tumors resistance to therapeutic drugs, Biotechnol. Bioeng. 116 (1) (2019) 206–226.

[2] Shawn P. Carey, Alina Starchenko, Alexandra L. McGregor, Cynthia A. Reinhart-King, Leading malignant cells initiate collective epithelial cell invasion in a three-dimensional heterotypic tumor spheroid model, Clin. Exp. Metastasis 30 (5) (2013) 615–630.

[3] Aleksandra Karolak, Dmitry A. Markov, Lisa J. McCawley, Katarzyna A. Rejniak, Towards personalized computational oncology: from spatial models of tumour spheroids, to organoids, to tissues, J. R. Soc. Interface 15 (138) (2018) 20170703.

[4] Lucia Le Roux, Dawid Schellingerhout, Andrei Volgin, David Maxwell, Katashi Ishihara, Juri Gelovani, Optimizing imaging of 3D multicellular tumor spheroids with fluorescent reporter proteins using confocal microscopy, Microsc. Microanal. 14 (S2) (2008) 734–735.

[5] Louis-Bastien Weiswald, Dominique Bellet, Virginie Dangles-Marie, Spherical cancer models in tumor biology, Neoplasia 17 (1) (2015) 1–15.

[6] Ibiayi Dagogo-Jack, Alice T. Shaw, Tumour heterogeneity and resistance to cancer therapies, Nat. Rev. Clin. Oncol. 15 (2) (2018) 81.

[7] Robert M. Sutherland, Cell and environment interactions in tumor microregions: the multicell spheroid model, Science 240 (4849) (1988) 177–184.

[8] Juergen Friedrich, Claudia Seidel, Reinhard Ebner, Leoni A. Kunz-Schughart, Spheroid-based drug screen: considerations and practical approach, Nat. Protoc. 4 (3) (2009) 309.

[9] Sritama Nath, Gayathri R. Devi, Three-dimensional culture systems in cancer research: Focus on tumor spheroid model, Pharmacol. Ther. 163 (2016) 94–108.

[10] Christoph Mark, Thomas J. Grundy, Pamela L. Strissel, David Böhringer, Nadine Grummel, Richard Gerum, Julian Steinwachs, Carolin C. Hack, Matthias W. Beckmann, Markus Eckstein, et al., Collective forces of tumor spheroids in three-dimensional biopolymer networks, Elife 9 (2020) e51912.

[11] Jose M. Ayuso, Haneen A. Basheer, Rosa Monge, Pablo Sánchez-Álvarez, Manuel Doblaré, Steven D. Shnyder, Victoria Vinader, Kamyar Afarinkia, Luis J. Fernández, Ignacio Ochoa, Study of the chemotactic response of multicellular spheroids in a microfluidic device, PLoS One 10 (10) (2015) e0139515.

[12] Ludivine Guillaume, Lise Rigal, Jérôme Fehrenbach, Childérick Severac, Bernard Ducommun, Valérie Lobjois, Characterization of the physical properties of tumor-derived spheroids reveals critical insights for pre-clinical studies, Sci. Rep. 9 (1) (2019) 1–9.

[13] Jiandong Wu, Xun Wu, Francis Lin, Recent developments in microfluidics-based chemotaxis studies, Lab Chip 13 (13) (2013) 2484–2499.

[14] Shing-Yi Cheng, Steven Heilman, Max Wasserman, Shivaun Archer, Michael L. Shuler, Mingming Wu, A hydrogel-based microfluidic device for the studies of directed cell migration, Lab Chip 7 (6) (2007) 763–769.

[15] Jose M. Ayuso, Rosa Monge, Guillermo A. Llamazares, Marco Moreno, Maria Agirregabiria, Javier Berganzo, Manuel Doblare, Iñaki Ochoa, Luis J. Fernandez, SU-8 based microdevices to study self-induced chemotaxis in 3D microenvironments, Front. Mater. 2 (2015) 37.

[16] Jose M. Ayuso, María Virumbrales-Muñoz, Alodia Lacueva, Pilar M. Lanuza, Elisa Checa-Chavarria, Pablo Botella, Eduardo Fernández, Manuel Doblare, Simon J. Allison, Roger M. Phillips, et al., Development and characterization of a microfluidic model of the tumour microenvironment, Sci. Rep. 6 (1) (2016) 1–16.

[17] Aliya Fatehullah, Si Hui Tan, Nick Barker, Organoids as an in vitro model of human development and disease, Nature Cell Biol. 18 (3) (2016) 246–254.

[18] Shi-Lei Xue, Bo Li, Xi-Qiao Feng, Huajian Gao, Biochemomechanical poroelastic theory of avascular tumor growth, J. Mech. Phys. Solids 94 (2016) 409–432.

[19] Pietro Mascheroni, Cinzia Stigliano, Melania Carfagna, Daniela P. Boso, Luigi Preziosi, Paolo Decuzzi, Bernhard A. Schrefler, Predicting the growth of glioblastoma multiforme spheroids using a multiphase porous media model, Biomech. Model. Mechanobiol. 15 (5) (2016) 1215–1228.

[20] H.P. Greenspan, On the growth and stability of cell cultures and solid tumors, J. Theoret. Biol. 56 (1) (1976) 229–242.

[21] H.M. Byrne, Mark A.J. Chaplain, Free boundary value problems associated with the growth and development of multicellular spheroids, European J. Appl. Math. 8 (6) (1997) 639–658.

[22] C.Y. Chen, H.M. Byrne, J.R. King, The influence of growth-induced stress from the surrounding medium on the development of multicell spheroids, J. Math. Biol. 43 (3) (2001) 191–220.

[23] D. Ambrosi, F. Mollica, On the mechanics of a growing tumor, Internat. J. Engrg. Sci. 40 (12) (2002) 1297–1316.

[24] D. Ambrosi, F. Mollica, The role of stress in the growth of a multicell spheroid, J. Math. Biol. 48 (5) (2004) 477–499.

[25] D. Ambrosi, Simone Pezzuto, Davide Riccobelli, T. Stylianopoulos, P. Ciarletta, Solid tumors are poroelastic solids with a chemo-mechanical feedback on growth, J. Elasticity 129 (1) (2017) 107–124.

[26] Massimiliano Fraldi, Angelo R. Carotenuto, Cells competition in tumor growth poroelasticity, J. Mech. Phys. Solids 112 (2018) 345–367.

[27] Joshua A. Bull, Franziska Mech, Tom Quaiser, Sarah L. Waters, Helen M. Byrne, Mathematical modelling reveals cellular dynamics within tumour spheroids, PLoS Comput. Biol. 16 (8) (2020) e1007961.

[28] M. Amereh, R. Edwards, M. Akbari, B. Nadler, In-silico modeling of tumor spheroid formation and growth, Micromachines 12 (2021) 749.

[29] Holger Perfahl, Barry D. Hughes, Tomás Alarcón, Philip K. Maini, Mark C. Lloyd, Matthias Reuss, Helen M. Byrne, 3D hybrid modelling of vascular network formation, J. Theoret. Biol. 414 (2017) 254–268.

[30] Jacobo Ayensa-Jiménez, Marina Pérez-Aliacar, Teodora Randelovic, Sara Oliván, Luis Fernández, José Antonio Sanz-Herrera, Ignacio Ochoa, Mohamed H. Doweidar, Manuel Doblaré, Mathematical formulation and parametric analysis of in vitro cell models in microfluidic devices: application to different stages of glioblastoma evolution, Sci. Rep. 10 (1) (2020) 1–21.

[31] Anna Kane Laird, Dynamics of tumour growth, Br. J. Cancer 18 (3) (1964) 490.

[32] Graeme J. Pettet, C.P. Please, M.J. Tindall, D.L.S. McElwain, The migration of cells in multicell tumor spheroids, Bull. Math. Biol. 63 (2) (2001) 231–257.

[33] Xin Lu, Yibin Kang, Hypoxia and hypoxia-inducible factors: master regulators of metastasis, Clin. Cancer Res. 16 (24) (2010) 5928–5935.

[34] A.S.G. Curtis, G.M. Seehar, The control of cell division by tension or diffusion, Nature 274 (5666) (1978) 52–53.

[35] P. Moreo, J.M. Garcia-Aznar, M. Doblare, Modeling mechanosensing and its effect on the migration and proliferation of adherent cells, Acta Biomater. 4 (2008) 613–621.

[36] J.A. Sanz-Herrera, P. Moreo, J.M. Garcia-Aznar, M. Doblare, On the effect of substrate curvature on cell mechanics, Biomaterials 30 (34) (2009) 6674–6686.

[37] Sui Huang, Donald E. Ingber, Cell tension, matrix mechanics, and cancer development, Cancer Cell 8 (3) (2005) 175–176.

[38] Anika Nagelkerke, Johan Bussink, Alan E. Rowan, Paul N. Span, The mechanical microenvironment in cancer: How physics affects tumours, in: Seminars in Cancer Biology, 35, Elsevier, 2015, pp. 62–70.

[39] Alicia Martínez-González, Gabriel F. Calvo, Luis A. Pérez Romasanta, Víctor M. Pérez-García, Hypoxic cell waves around necrotic cores in glioblastoma: a biomathematical model and its therapeutic implications, Bull. Math. Biol. 74 (12) (2012) 2875–2896.

[40] Daniel J. Brat, Glioblastoma: biology, genetics, and behavior, in: American Society of Clinical Oncology Educational Book, Vol. 32, No. 1, American Society of Clinical Oncology, 2012, pp. 102–107.

[41] David Robert Grimes, Catherine Kelly, Katarzyna Bloch, Mike Partridge, A method for estimating the oxygen consumption rate in multicellular tumour spheroids, J. R. Soc. Interface 11 (92) (2014) 20131124.

[42] Hongmei Yu, Janna Kay Mouw, Valerie M. Weaver, Forcing form and function: biomechanical regulation of tumor evolution, Trends Cell Biol. 21 (1) (2011) 47–56.

[43] David Lacalle, Héctor Alfonso Castro-Abril, Teodora Randelovic, César Domínguez, Jónathan Heras, Eloy Mata, Gadea Mata, Yolanda Méndez, Vico Pascual, Ignacio Ochoa, SpheroidJ: An open-source set of tools for spheroid segmentation, Comput. Methods Programs Biomed. 200 (2021) 105837.

[44] Priya R. Baraniak, Todd C. McDevitt, Scaffold-free culture of mesenchymal stem cell spheroids in suspension preserves multilineage potential, Cell Tissue Res. 347 (2012) 701–711.

[45] Ian F. Tannock, Oxygen diffusion and the distribution of cellular radiosensitivity in tumours, Br. J. Radiol. 45 (535) (1972) 515–524.

[46] Brian W. Pogue, Julia A. O'Hara, Carmen M. Wilmot, Keith D. Paulsen, Harold M. Swartz, Estimation of oxygen distribution in RIF-1 tumors by diffusion model-based interpretation of pimonidazole hypoxia and Eppendorf measurements, Radiat. Res. 155 (1) (2001) 15–25.

[47] Peggy L. Olive, Charlene Vikse, Martin J. Trotter, Measurement of oxygen diffusion distance in tumor cubes using a fluorescent hypoxia probe, Int. J. Radiat. Oncol. Biol. Phys. 22 (3) (1992) 397–402.

[48] Christina H. Wang, Jason K. Rockhill, Maciej Mrugala, Danielle L. Peacock, Albert Lai, Katy Jusenius, Joanna M. Wardlaw, Timothy Cloughesy, Alexander M. Spence, Russ Rockne, et al., Prognostic significance of growth kinetics in newly diagnosed glioblastomas revealed by combining serial imaging with a novel biomathematical model, Cancer Res. 69 (23) (2009) 9133–9140.

[49] Abramo Agosti, Clara Cattaneo, Chiara Giverso, Davide Ambrosi, Pasquale Ciarletta, A computational framework for the personalized clinical treatment of glioblastoma multiforme, ZAMM Z. Angew. Math. Mech. 98 (12) (2018) 2307–2327.

[50] Philip Gerlee, Alexander R.A. Anderson, An evolutionary hybrid cellular automaton model of solid tumour growth, J. Theoret. Biol. 246 (4) (2007) 583–603.

[51] Abramo Agosti, Chiara Giverso, Elena Faggiano, Aymeric Stamm, Pasquale Ciarletta, A personalized mathematical tool for neuro-oncology: A clinical case study, Int. J. Non-Linear Mech. 107 (2018) 170–181.

[52] Corinne E. Griguer, Claudia R. Oliva, Eric Gobin, Pascale Marcorelles, Dale J. Benos, Jack R. Lancaster Jr., G. Yancey Gillespie, CD133 is a marker of bioenergetic stress in human glioma, PLoS One 3 (11) (2008) e3655.

[53] Alicia Martínez-González, Mario Durán-Prado, Gabriel F. Calvo, Francisco J. Alcaín, Luis A. Pérez-Romasanta, Víctor M. Pérez-García, Combined therapies of antithrombotics and antioxidants delay in silico brain tumour progression, Math. Med. Biol. 32 (3) (2015) 239–262.

[54] H.M. Byrne, T. Alarcon, M.R. Owen, S.D. Webb, P.K. Maini, Modelling aspects of cancer dynamics: a review, Phil. Trans. R. Soc. A 364 (1843) (2006) 1563–1578.
[55] Jane S. Tjia, Prabhas V. Moghe, Regulation of cell motility on polymer substrates via" dynamic," cell internalizable, ligand microinterfaces, Tissue Eng. 8 (2) (2002) 247–261.
[56] Brian Stramer, Roberto Mayor, Mechanisms and in vivo functions of contact inhibition of locomotion, Nature Rev. Mol. Cell. Biol. 18 (1) (2017) 43–55.
[57] M.R.K. Mofrad, R.D. Kamm, Continuum Elastic or Viscoelastic Models for the Cell, Cambridge University Press, 2006,
[58] T. Sussman, K.J. Bathe, A model of incompressible isotropic hyperelastic material behavior using spline interpolations of tension–compression test data, Commun. Numer. Meth. Eng. 25 (2009) 53–63.
[59] M. Latorre, F.J. Montans, Extension of the Sussman–Bathe spline-based hyperelastic model to incompressible transversely isotropic materials, Comput. Struct. 122 (2013) 13–26.
[60] M. Latorre, F.J. Montans, On the interpretation of the logarithmic strain tensor in an arbitrary system of representation, Int. J. Solids Struct. 51 (2014) 1507–1515.
[61] Katarzyna S. Kopanska, Yara Alcheikh, Ralitza Staneva, Danijela Vignjevic, Timo Betz, Tensile forces originating from cancer spheroids facilitate tumor invasion, PLoS One 11 (6) (2016) e0156442.
[62] Chiara Giverso, Luigi Preziosi, Influence of the mechanical properties of the necrotic core on the growth and remodelling of tumour spheroids, Int. J. Non-Linear Mech. 108 (2019) 20–32.
[63] O.C. Zienkiewicz, Robert L. (Robert Leroy) Taylor, The Finite Element Method, Butterworth–Heinemann, 2000.
[64] J.A. Sanz-Herrera, J. Barrasa-Fano, M. Condor, H. Van Oosterwyck, Inverse method based on 3D nonlinear physically constrained minimisation in the framework of traction force microscopy, Soft Matter 17 (2021) 10210–10222.
[65] J. Barrasa-Fano, A. Shapeti, J. De Jong, A. Ranga, H. Sanz-Herrera, Advanced in silico validation framework for three-dimensional traction force microscopy and application to an in vitro model of sprouting angiogenesis, Acta Biomater. 126 (2021) 326–338.
[66] Richard M. Enmon Jr., Kim C. O'Connor, Daniel J. Lacks, Daniel K. Schwartz, Robert S. Dotson, Dynamics of spheroid self-assembly in liquid-overlay culture of DU 145 human prostate cancer cells, Biotechnol. Bioeng. 72 (6) (2001) 579–591.
[67] Meitham Amereh, Roderick Edwards, Mohsen Akbari, Ben Nadler, In-silico modeling of tumor spheroid formation and growth, Micromachines 12 (7) (2021) 749.
[68] I. Smyrek, B. Mathew, S.C. Fischer, S.M. Lissek, S. Becker, E.H.K. Stelzer, E-cadherin, actin, microtubules and FAK dominate different spheroid formation phases and important elements of tissue integrity, Biol. Open 8 (1) (2019) bio037051.
[69] Stephanie Eugenie Brigitte McArdle, Kinana Habra, Joshua R.D. Pearson, Swift formation of optimal single spheroids towards in-vitro 3-dimensional tumour models, 2021, bioRxiv.
[70] X. Cui, Y. Hartanto, H. Zhang, Advances in multicellular spheroids formation, J. R. Soc. Interface 14 (127) (2017) 20160877.
[71] Ruei-Zeng Lin, Li-Fang Chou, Chi-Chen Michael Chien, Hwan-You Chang, Dynamic analysis of hepatoma spheroid formation: roles of E-cadherin and β1-integrin, Cell Tissue Res. 324 (3) (2006) 411–422.
[72] Jiangping Xu, Guillermo Vilanova, Hector Gomez, A mathematical model coupling tumor growth and angiogenesis, PLoS One 11 (2) (2016) e0149422.
[73] Abdullah Chandra Sekhar Talari, Ahtasham Raza, Shazza Rehman, Ihtesham U. Rehman, Analyzing normal proliferating, hypoxic and necrotic regions of T-47D human breast cancer spheroids using Raman spectroscopy, Appl. Spectrosc. Rev. 52 (10) (2017) 909–924.
[74] Hezhen Li, Bingxi Lei, Wei Xiang, Hai Wang, Wenfeng Feng, Yawei Liu, Songtao Qi, Differences in protein expression between the U251 and U87 cell lines, Turk Neurosurg 27 (6) (2017) 894–903.